Bulletin of the Earthquake
Research Institute
University of Tokyo
Vol. 59 (1984) pp. 1-51

*Focal Mechanisms and Spatial Distribution of Intermediate-depth Earthquakes beneath the Kanto District and Vicinity with Relation to the Double Seismic Planes**

Tadashi Maki

Earthquake Research Institute, University of Tokyo

(Received January 31, 1984)

Abstract

The slab intersection of the Northeast Honshu and Izu-Bonin Arcs beneath Central Japan is modeled from the depth contours of hypocenter distributions of intermediate-depth earthquakes relocated by correcting the Pn station biases. The Northeast Honshu slab bends strongly to the northwest beneath the Kanto District. Intense clusters of subcrustal hypocenters beneath the western part of Ibaraki and Chiba Prefectures are located within the highly stressed region of the Northeast Honshu slab due to intersection with the Izu-Bonin slab. A separation of the inclined seismic zone into double layers is seen for the Northeast Honshu slab from a relatively deeper layer of hypocenters, but the double layers are not seen for the Izu-Bonin slab. A separation of 30 km between the upper and lower seismic layers is estimated from the hypocenters beneath the Kanto District by the JHD method. Fault-plane solutions are obtained for 144 out of 286 intermediate-depth earthquakes which occurred at depths of h=80-200 km with magnitudes of 4.0 or more during the period from 1963 to 1980. Intermediate-depth earthquakes located on the inland side show the down-dip compression, and the down-dip extension is observed on the Pacific side. The strike-slip, normal fault and hinge fault, which are different from the down-dip types of focal mechanisms, are also observed for intermediate-depth earthquakes in and around the Kanto District. Intermediate-depth earthquakes with reverse faults are located along the Pacific coast, and other types are observed for earthquakes on the Japan Sea side and off Miyagi and Fukushima Prefectures. The strike-slip is predominant for earthquakes beneath the central part of the Kanto District and these are located along a contact plane of the southwestern end of the Northeast Honshu slab with the northern end of the Izu-Bonin slab.

* Read on April, 19, 1983, at the monthly meeting (Danwakai) of the Earthquake Research Institute.

1. Introduction

The double seismic layers were first observed in the Kanto District (Fig. 1) by TSUMURA (1973) on the depth distribution of small and micro-earthquakes located by the recent high-sensitivity seismograph network of the Earthquake Research Institute (ERI). However, no studies have been followed for detailed features of spatial distribution of hypocenters and focal mechanisms related to the double seismic planes beneath the Kanto District. In Northeast Japan the spatial distribution of hypocenters and focal mechanisms have been extensively studied with relation to the double seismic layers (UMINO and HASEGAWA, 1975, 1982; HASEGAWA *et al.*, 1978a, b, 1979; TAKAGI *et al.*, 1977; YOSHII, 1979). A thin two-layered structure is found for the micro-earthquakes located by the Tohoku University network and for larger earthquakes relocated using The Japan Meterological Agency (JMA) travel-time data (UMINO and HASEGAWA, 1975, 1982). The systematic difference of focal mechanisms was also shown between the upper and lower layers of the double seismic planes (UMINO and HASEGAWA, 1975; HASEGAWA *et al.*, 1978a). They showed the down-dip compression for earthquakes along the upper plane and the down-dip extension along the lower plane. The double seismic planes below Northeast Japan are observed at depths from 80 to 150 km, and the separation between the upper and lower planes is estimated to be 30 km (UMINO and HASEGAWA, 1975, 1982). The upper plane of the double seismic zone was found to coincide with the conversion plane of ScS to ScSp wave (OKADA, 1971, 1979) from the time differences between the two phases (HASEGAWA *et al.*, 1979).

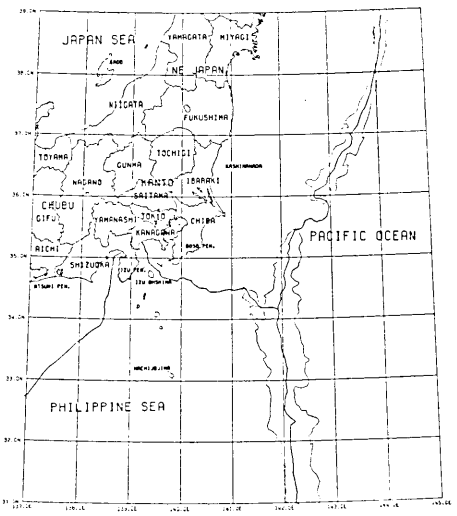

Fig. 1. Location map of the Kanto District and vicinity, Central Japan. The plate boundaries identified from the trench and trough axes are shown by thick lines, and thin lines denote bathymetric contours of 7000 m.

Some speculative models have been introduced for the two types of focal mechanisms along the double seismic planes, namely the un-

bending of descending slab (ENGDAHL and SCHOLZ, 1977), sagging of slab (SLEEP, 1979), and thermal stress (GOTO and HAMAGUCHI, 1983). These models should be applicable to any descending slabs in the worlds, but there are some regions of inclined seismic zones without double seismic layers (FUJITA and KANAMORI, 1981). And some confused patterns of focal mechanisms are observed from the fault-plane solutions given by UMINO and HASEGAWA (1975). Earthquakes in the deeper half of the inclined seismic zone show the separation of focal mechanisms into two types, but the focal mechanisms are variable for earthquakes in the shallower half. FUJITA and KANAMORI (1981) preferred the "in-plane" stresses to the "down-dip" stresses from the global survey of individual fault-plane solutions of intermediate-depth earthquakes. REYNERS and COLES (1982) showed a rather confused pattern of fault-plane solutions for intermediate-depth earthquakes beneath the Shumagin Islands, Alaska.

Recently focal mechanisms of intermediate-depth earthquakes were studied with relation to the spatial distribution of hypocenters in several areas in the world; the Banda Sea by CARDWELL and ISACKS (1978), the South Atlantic and Scotia Sea by FORSYTH (1975), the New Hebrides Island Arc by PASCAL *et al.* (1978), Chile by STAUDER (1973), Peru (the Nazca Plate) by STAUDER (1975), the Lesser Antilles Arc by STEIN *et al.* (1982) and DOREL (1981), the Kurile Arc by VEITH (1974, 1977) and STAUDER and MUALCHIN (1976) and Japan by AOKI (1974), SASATANI (1976) and SHIONO *et al.* (1980). Global surveys of focal mechanisms for intermediate-depth earthquakes were made by ISACKS (1968), ISACKS and MOLNAR (1971), ISACKS and BARAZANGI (1977) and FUJITA and KANAMORI (1981).

Two types of focal mechanisms of the down-dip compression and extension along the inclined seismic zone have also been observed for the intermediate-depth earthquakes in the Kurile-Kamchatka region (ISACKS and MOLNAR, 1971; VEITH, 1974; STAUDER and MUALCHIN, 1976). ISACKS and BARAZANGI (1977) showed the separation of focal mechanisms into two types at the top and bottom of slabs for the Kurile-Kamchatka and Peru regions. The presence of these two types of focal mechanisms leads one to wonder about the simple gravitational sinking model of the slabs (ISACKS and MOLNAR, 1971). They interpreted these two types as the volume change across the olivine-spinel phase transition boundary. A systematic difference of focal mechanisms of intermediate-depth earthquakes was observed in azimuths of the nearly vertical nodal plane from NE-SW in the Kurile-Kamchatka Arc to E-W in the Hokkaido Arc (STAUDER and MUALCHIN, 1976). Such a variation of focal mechanisms is interpreted as the slab contortion under the lateral extension or the tearing of slab by the

hinge faulting in the Hokkaido Corner. An axial extension along the descending slab was observed for intermediate-depth earthquakes in the northernmost part of Chile, but in the southern extremity a hinge faulting was observed (STAUDER, 1973). Only the extension along the seismic zone was found for intermediate-depth earthquakes under Peru (STAUDER, 1975). STUDER interpreted this type of the focal mechanism as the stress guide, representing the failure under the gravitational sinking of the slab. He also mentioned the depth variation of azimuths of tension axes from the horizontal E-W extension for the shallower foci to the northeastward dipping extension for the deeper foci.

For intermediate-depth earthquakes in the South Sandwich Arc the down-dip extension is observed in the northern part and the down-dip compression in the southern part (FORSYTH, 1975). Forsyth interpreted this regional change of stress pattern by the faster descent of the younger southern half of the subducted South America Plate. For the northern end of the arc the hinge faulting was also observed. Besides the down-dip extension along the seismic zone, a focal mechanism with the vertical nodal plane was observed in the New Hebrides Island Arc (PASCAL *et al.*, 1978). This vertical nodal plane is parallel to a transverse feature of the hypocenter distribution and the northern scarp of the d'Entrecasteaux fracture zone. A regional variation of stresses along the inclined seismic zone was also observed for the Banda Sea Arc (CARDWELL and ISACKS, 1978).

SUZUKI *et al.* (1981, 1983) showed the double seismic planes in the Hokkaido region. They suggested more active occurrence of intermediate-depth earthquakes along the lower plane than along the upper plane. SAMOWITZ and FORSYTH (1981) showed a focal mechanism of the down-dip extension for an earthquake which occurred in the northern Marianas. NISHIDE *et al.* (1982) also showed the double seismic planes in Northeast Japan and other regions in Japan from the relocated earthquakes from 1963 to 1980. The N-S striking extension observed for microearthquakes at intermediate-depth beneath the Kanto District (UKAWA and IMOTO, 1982) suggests a lateral segmentation of the descending slabs. MIZOUE *et al.* (1982) showed the reflected wave at the lower plane which suggests a seaward extension of the two-layered structure of the seismic zone. STEFANI *et al.*, (1982) also showed a separation of 38 ± 5 km between the upper boundary of the slab and the seismic zone beneath the Kurile Islands.

BARAZANGI and ISACKS (1979) compared the spatial distribution of intermediate-depth earthquakes which are located by the local and teleseismic data in Northeast Japan and the Aleutian Islands. They pointed out the large effect of the location techniques and the earth's

velocity structure around the slabs. MAKI (1982a) studied the effects of station coverage (distance and azimuth) around epicenters and the effects of errors in observed travel times for the locations of intermediate-depth earthquakes using the local travel-time data in Central Japan.

The hinge faulting between the Northeast Honshu and the Izu-Bonin slabs was observed for the deep earthqquakes beneath the Takayama region (AOKI, 1974). The hinge faulting between the Kurile and Northeast Japan slabs was also found by SASATANI (1976) from the mantle earthquakes beneath the Hokkaido region. SASATANI pointed out the predominance of the down-dip extension in the Hokkaido region and the down-dip compression on the Northeast Honshu side. A regional difference of focal mechanisms in the Kyushu-Ryukyu region was shown by SHIONO *et al.* (1980), namely the more sharply dipping seismic zone with the down-dip extension in the northern half and the more gently dipping ones with the down-dip compression in the southern half.

Various types of focal mechanism have been observed for intermediate-depth earthquakes in the world. Two types of the axial stress along the inclined seismic zone are observed at different depths or parts of the active regions with close relation to the spatial distribution of hypocenters. The configuration of the Northeast Honshu and Izu-Bonin slabs will be studied in the next chapter from the spatial distribution of relocated intermediate-depth earthquakes. In Chapter 3 focal mechanisms will be analyzed for intermediate-depth earthquakes which occurred during the period from 1963 to 1980. In Chapter 4 the spatial variation of focal mechanisms will be studied in comparison to the hypocenter distribution.

2. Spatial distribution of intermediate-depth earthquakes

The spatial distribution of intermediate-depth earthquakes is one bit of the basic data for medeling the configuration of descending slabs. The distribution of velocity and attenuation factor of seismic waves are not enough to reveal the slab configuration. Microearthquakes occurring at intermediate-depths beneath the Kanto District show the double seismic planes even for a short period (TSUMURA, 1973), but these data are effective for only a limited area directly beneath the Kanto District. On the other hand the hypocenters of larger earthques located by the JMA routine do not show such a double-layered structure due to bigger errors in hypocenter locations, epecially in focal depth, and to an insufficient number of earthquakes. In this chapter the double seismic planes are located from the relocated hypocenters

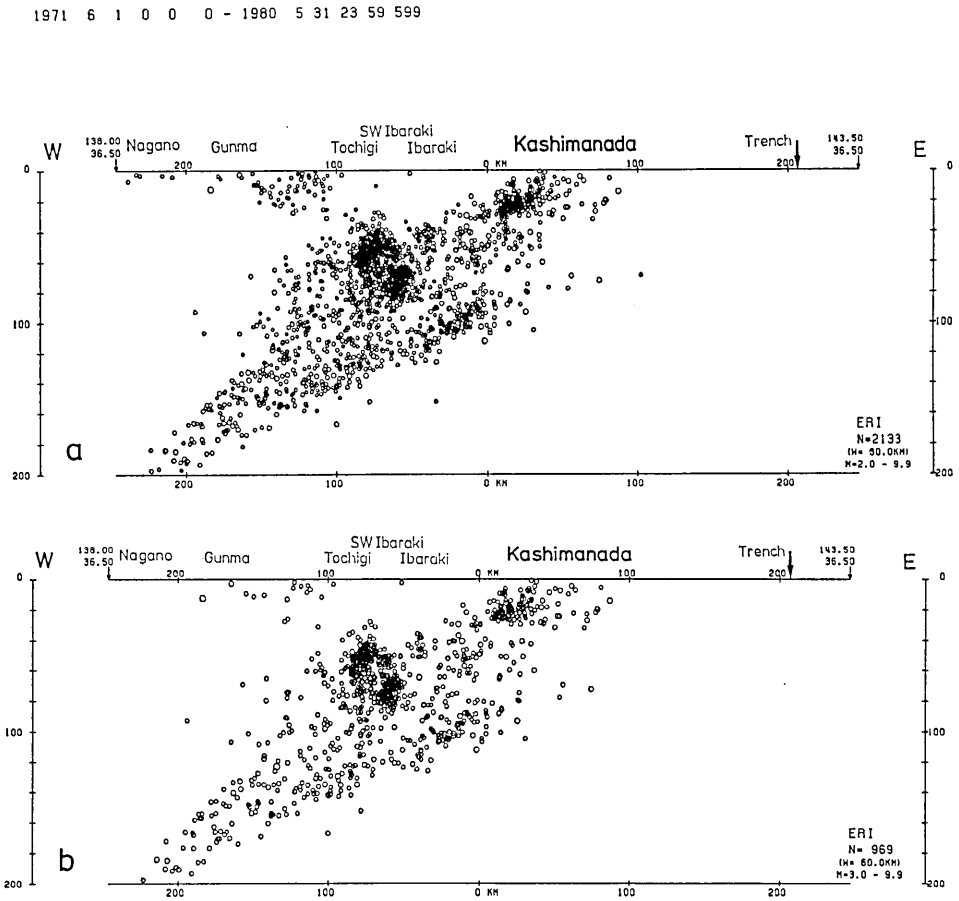

Fig. 2. Double seismic planes of the small and micro-earthquakes at intermediate-depths along the E-W section of the 120 km width between the two points (36.5°N, 138.0°E) and (36.5°N, 143.5°E), (a) smaller earthquakes with magnitudes down to 2.0 (n=2133), and (b) larger earthquakes with magnitudes of 3.0 or more (n=969). Hypocenters are taken from the ERI data located by the high-sensitivity seismograph network of the Kanto District (TSUMURA, 1973' 1981; TSUMURA and KARAKAMA, 1981) during the period from June of 1971 to May of 1980.

of intermediate-depth earthquakes by correcting the JMA travel times with the Pn station biases (MAKI, 1981a, b).

Fig. 2 shows the depth distributions of small and microearthquakes located by the ERI network along the E-W section from 36° to 37°N during the period from June of 1971 to May of 1980. The upper (a) includes smaller earthquakes down to a magnitude of 2.0, which are selected on the basis of the location criteria (five or more stations and errors less than 7.5 km). The lower (b) included larger earthquakes with magnitudes of 3.0 or more. The latter is prepared for comparison with the relocated hypocenters of larger earthquakes using

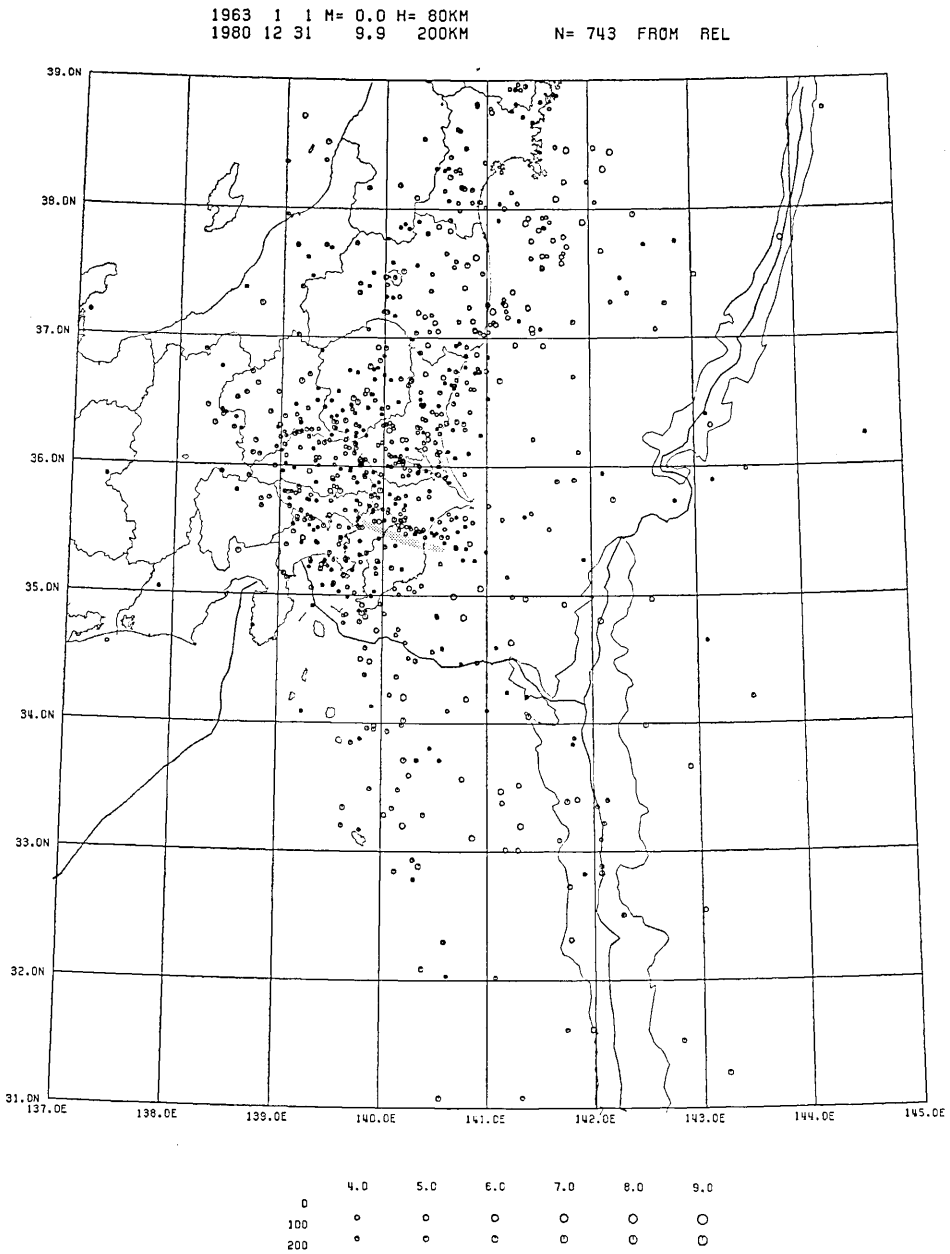

Fig. 3. Epicenter distribution of relocated intermediate-depth earthquakes (n=743) in and around the Kanto District, which occurred at depths from 80 to 200 km during the 18 years from 1963 to 1980. Hypocenters and origin times are determined by correcting the JMA travel-time data with the Pn station biases (MAKI, 1981a). Earthquake magnitudes are taken from JMA. Depth and magnitudes are denoted by different symbols as shown in the legend. The hatched area denotes a linear alignment of epicenters beneath the Boso Peninsula.

the JMA travel-time data (MAKI, 1981a). The double seismic planes have been shown in the depth distributions of microearthquakes in narrow sections about 20 km wide (TSUMURA, 1981; TSUMURA and KARAKAMA, 1981). Although the depth sections are as wide as 1° in Fig. 2, the hypocenters along the lower plane of the double seismic zone can be observed for depths from 80 to 160 km. A seaward extension of the lower plane is observed from a few earthquakes at depths shallower than 80 km beneath Kashimanada. The upper plane of the double seismic zone is disturbed by the intense clusters of hypocenters beneath the southwestern part of Ibaraki Prefecture. The separation and depth range of the double seismic planes are variable for other sections.

Fig. 3 shows the relocated epicenters of relatively large intermediate-depth earthquakes which occurred at depths from 80 to 200 km during the period from 1963 to 1980 with magnitudes of 4.0 or more ($n=743$). These earthquakes are located by correcting the JMA travel-time data with the Pn station biases (MAKI, 1981a). Earthquake magnitudes by JMA and focal depths are classified by different symbols. A linear pattern of epicenters beneath the middle part of Chiba Prefecture is denoted by hatching. These relocated earthquakes cover a wider area of the Kanto District and vicinity including the Japan Trench and Izu-Bonin Islands, in comparison with a small area directly beneath the Kanto District for the earthquakes located by the ERI network.

The seismic zone beneath the Kanto District shows a complicated pattern of hypocenter distribution (MAKI *et al.*, 1980). Here epicenter distributions for different ranges of focal depth and depth distributions for different sections will be used for modeling the configuration of the seismic zone. Epicenter distributions of intermediate-depth earthquakes are shown for every 20 km of focal depths from 40 to 200 km. The western extremities of epicenters are observed better than the eastern and they are useful to identity the upper boundary of the inclined seismic zone. Such clear boundaries on the western side tend to rule out another seismic zone inclined from the west. Some intensely active regions are found within or along the boundary of the seismic zone, such as those beneath the southwestern part of Ibaraki Prefecture, the middle part of Chiba Prefecture and beneath Kashimanada. Depth contours of the western end of the seismic zone are drawn by smoothing on epicenter maps for every 20 km depth, and they are shown by thick lines in Figs. 4a to h. The earthquakes in the southwestern end of Ibaraki Prefecture and Kashimanada, which show some systematic alignments of hypocenters, may be related to the interaction of the Pacific Plate and the overriding plate.

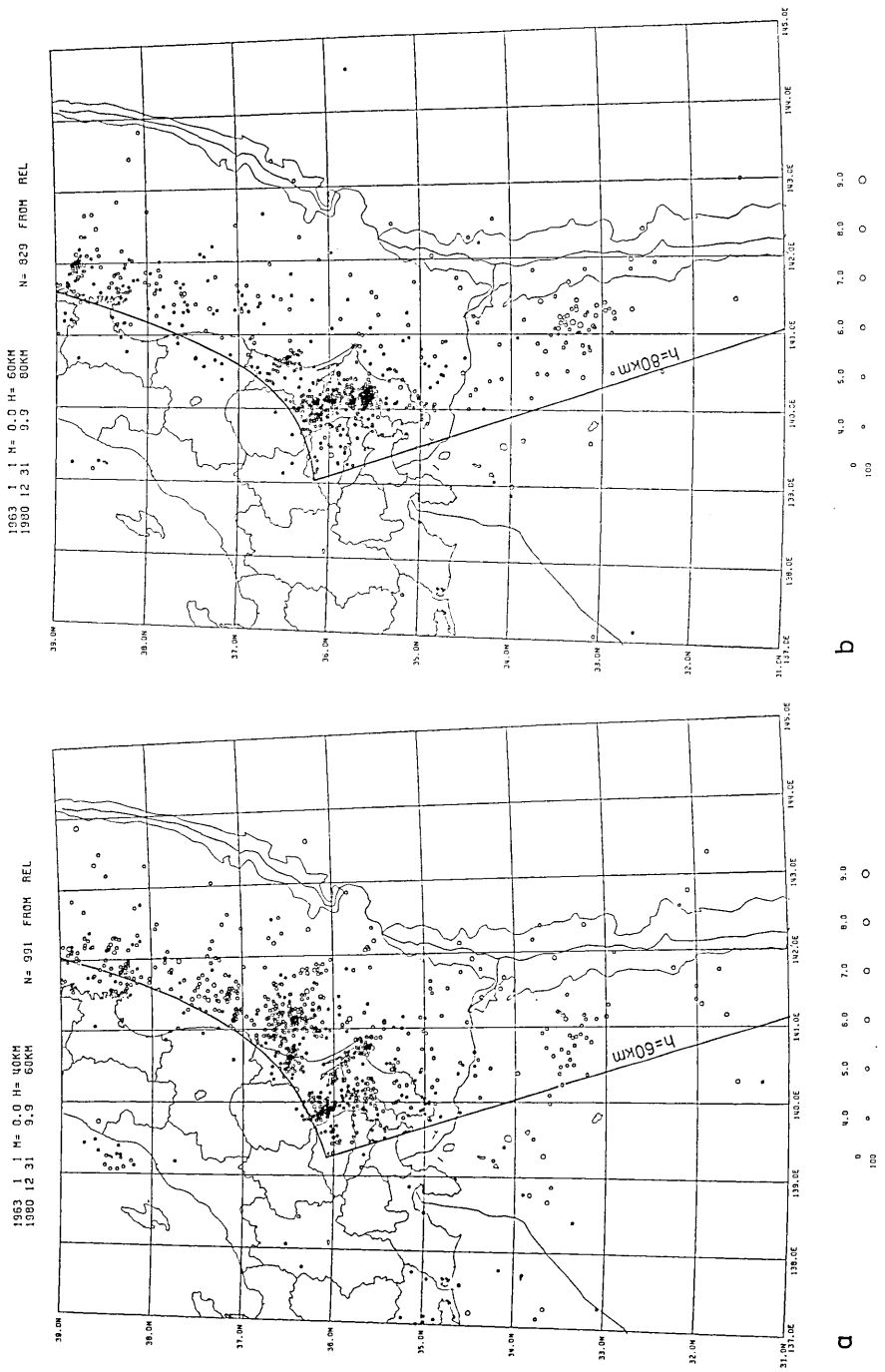
1963 1 1 M= 0.0 H= 40KM
1980 12 31 9.9 60KM
N= 991 FROM REL
h=60km
a
1963 1 1 M= 0.0 H= 60KM
1980 12 31 9.9 80KM
N= 829 FROM REL
h=80km
b

Fig. 4. a–b

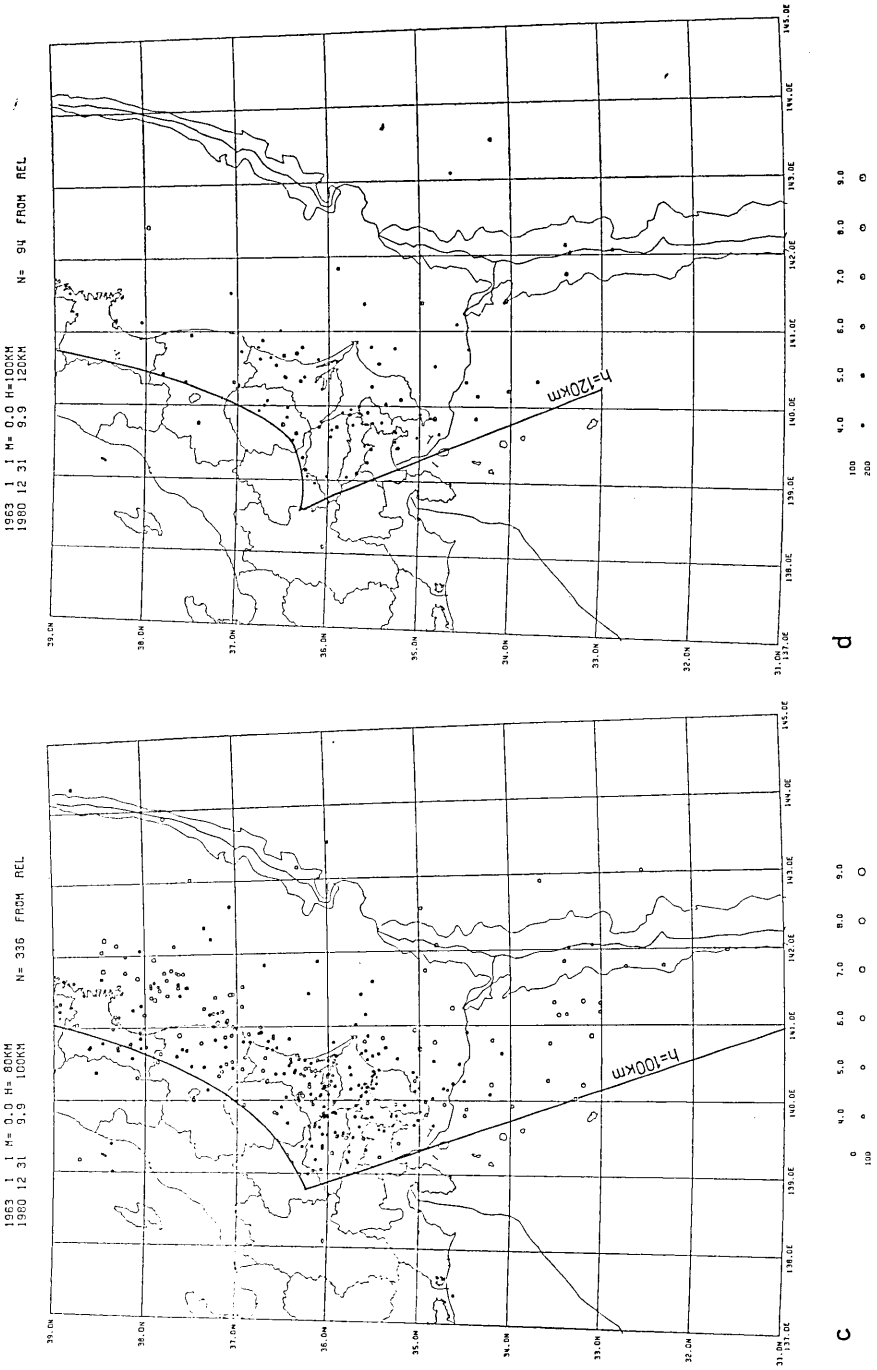
1963 1 1 M= 0.0 H=100KM N= 94 FROM REL
1980 12 31 9.9 120KM
h=120km
1963 1 1 M= 0.0 H= 80KM N= 336 FROM REL
1980 12 31 9.9 100KM
h=100km
d
c

Fig. 4. c–d

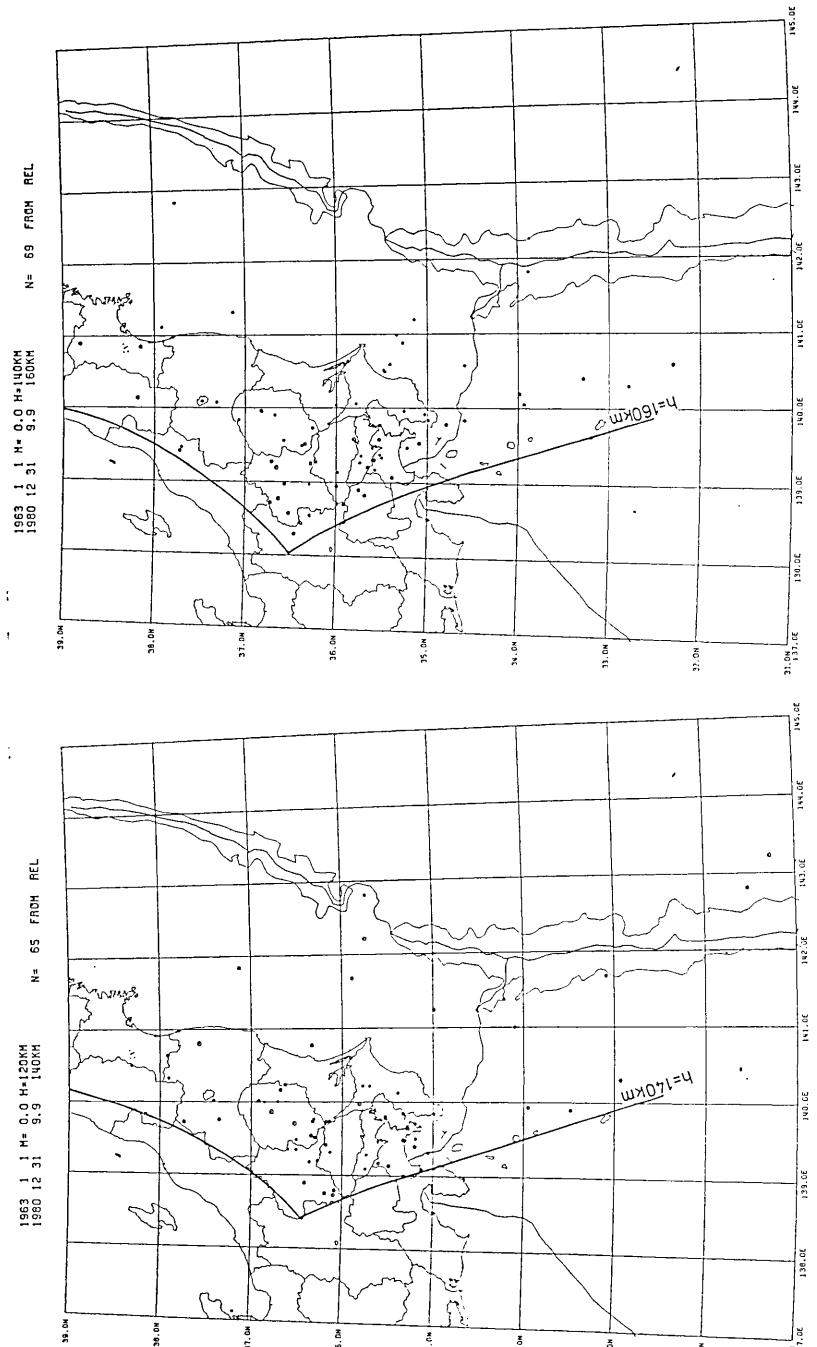
1963 1 1 M= 0.0 H=140KM
1980 12 31 9.9 160KM
N= 69 FROM REL
h=160km
1963 1 1 M= 0.0 H=120KM
1980 12 31 9.9 140KM
N= 65 FROM REL
h=140km
e
f

Fig. 4. e-f

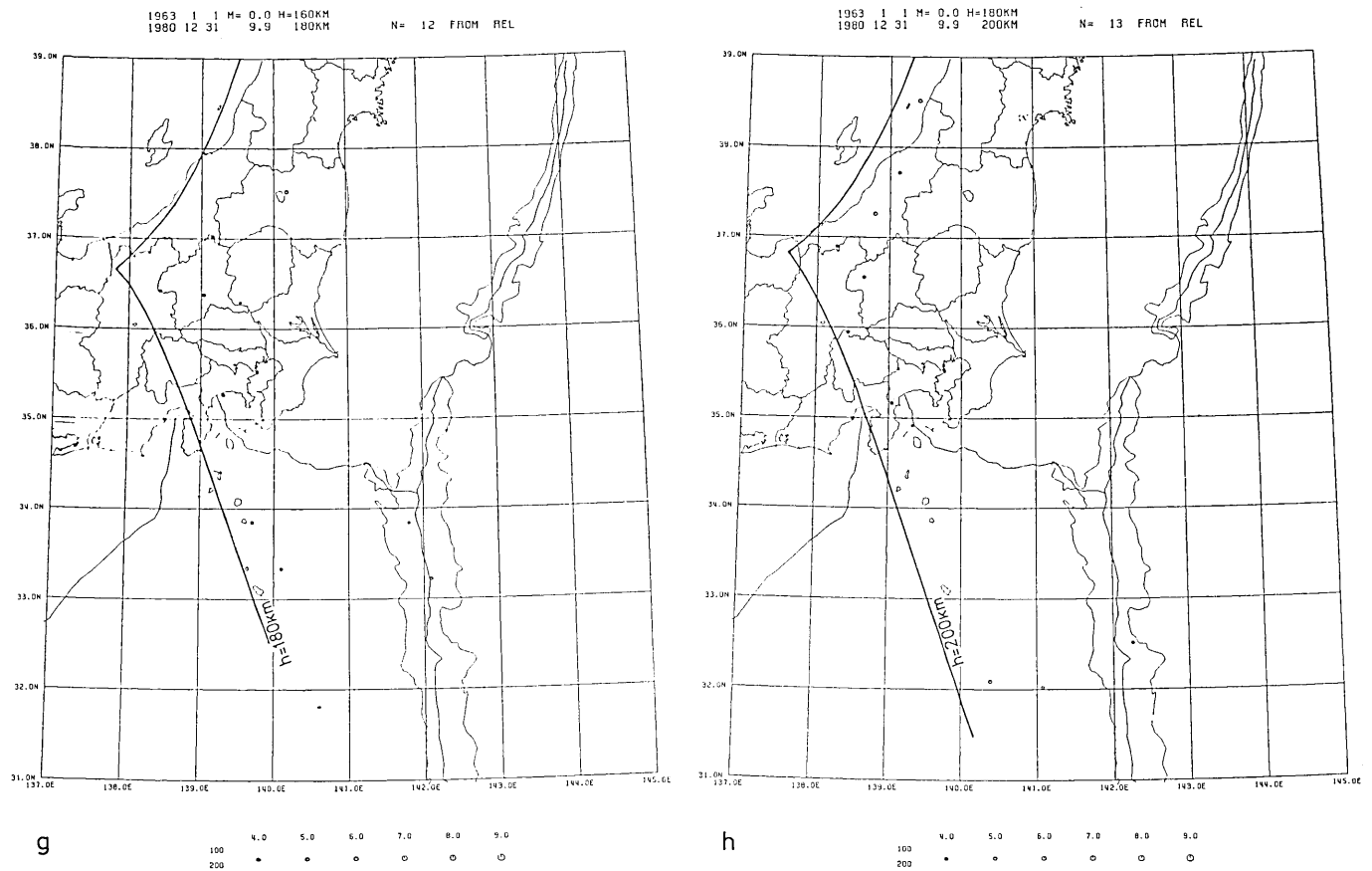

Fig. 4. Epicenter distributions of the relocated intermediate-depth earthquakes for different ranges of focal depth; (a) h=40~60 km (n=991), (b) h=60~80 km (n=829), (c) h=80~100 km (n=336), (d) h=100~120 km (n=94), (e) h=120~140 km (n=65), (f) h=140~160 km (n=69), (g) h=160~180 km (n=12), and (h) h=180~200 km (n=13). Thick lines denote the western extremities of epicenters for each range of focal depths, showing the upper boundary of the seismic zone inclined to the west.

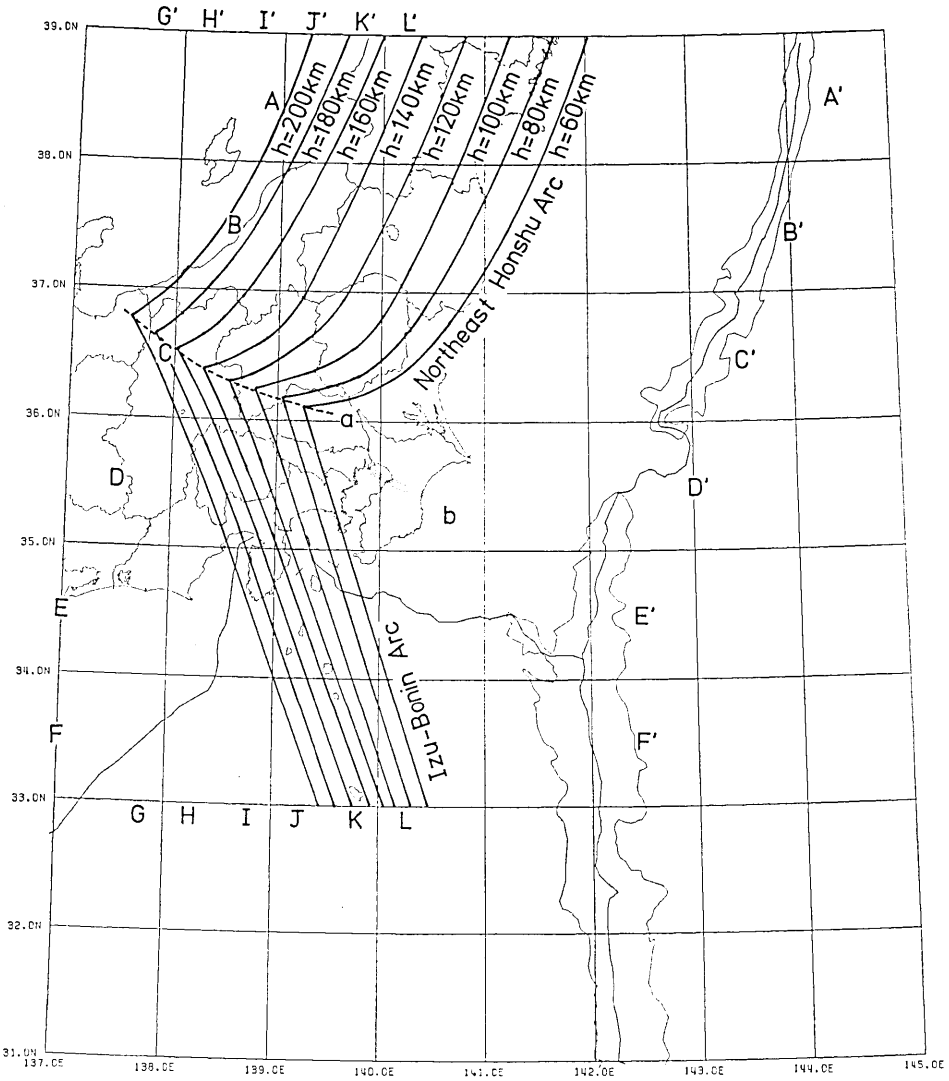

Fig. 5. Summary of the depth contours (thick lines) for every 20 km of the relocated intermediate-depth earthquakes in and around the Kanto District. The broken line (a) denotes the contact plane of the Northeast Honshu and Izu-Bonin slabs. The hatched area denotes the linear alignment of epicenters beneath the Boso Peninsula. Locations of the E-W and N-S sections of depth distributions are also shown (AA′ to LL′).

The earthquakes beneath the middle part of Chiba Prefecture are not located along the upper boundary of the Pacific Plate. Actual locations of hypocenters show some oozy patterns due to location errors, especially south off the Boso Peninsula near Hachijojima Island. Other depth contours with discontinuous features may be possible as observed

in the epicenter distribution of small and micro-earthquakes located by the ERI network.

Fig. 5 summarizes the depth contours of upper boundaries of the inclined seismic zone. The disruptive feature of the depth contours in Central Japan are also seen on the ISC epicenter map by UTSU (1974). The Northeast Honshu slab dips at an angle of 30° and the Izu-Bonin slab shows a greater dipping angle of 60° (ISACKS *et al.*, 1968). The two slabs have contact as shown by a broken line (a), accompanying a strong northwestward bending at the shallower part of the Northeast Honshu slab. The linear alignment of epicenters beneath the middle part of Chiba Prefecture shown in Fig. 3 is reproduced as the hatched area "b". The present depth contours are consistent with the geographical pattern of the Quaternary compressive deformation (MATSUDA, 1978), volcanic front (SUGIMURA, 1960) and metamorphic belts in the Kanto District (MIYASHIRO, 1961). The contact plane between the two slabs parallels the Sagami Trough and may be extended to distorted bathymetric contours of 7000 m of the Japan Trench near the point D, and also to the source region of Takayama deep-focus earthquakes with the strike-slip at the depth of about 300 km (AOKI, 1974).

The intersection of the two slabs has been studied from the spatial distribution of hypocenters and focal mechanisms for the Hokkaido Corner (SASATANI, 1976; STAUDER and MUALCHIN, 1976; MORIYA, 1978), the Central Honshu (ISACKS *et al.*, 1968; ISACKS and MOLNAR, 1971; AOKI, 1974) and the Ryukyu-Taiwan region (SHIONO *et al.*, 1980). The systematic variation of focal mechanisms around the junctions are commonly observed in these regions. The focal mechanism with the northward extension is observed in the Hokkaido region as well as the westward compression in the Northeast Honshu slab. At the boundaries of the Kurile and Northeast Honshu slabs the hinge faulting is observed.

The double seismic planes have been observed on the depth distribution of earthquake hypocenters along the narrow sections including a number of hypocenters (TSUMURA, 1973, 1981; TSUMURA and KARAKAMA, 1981). Such narrow sections are not usable for large earthquakes because of the smaller number of hypocenters. Fig. 6 shows the depth distribution of the relocated earthquakes along the E-W sections of a width of 55 km on each side (AA′ to FF′ in Fig. 5). Earthquake magnitudes are shown by different sized circles. Shaded areas denote possible positions of upper boundaries of the inclined seismic zone derived from the depth contours in Fig. 5. For the northern sections (AA′, BB′ and CC′) the seismic zone inclined to the west can be traced down to a depth of about 200 km. For the

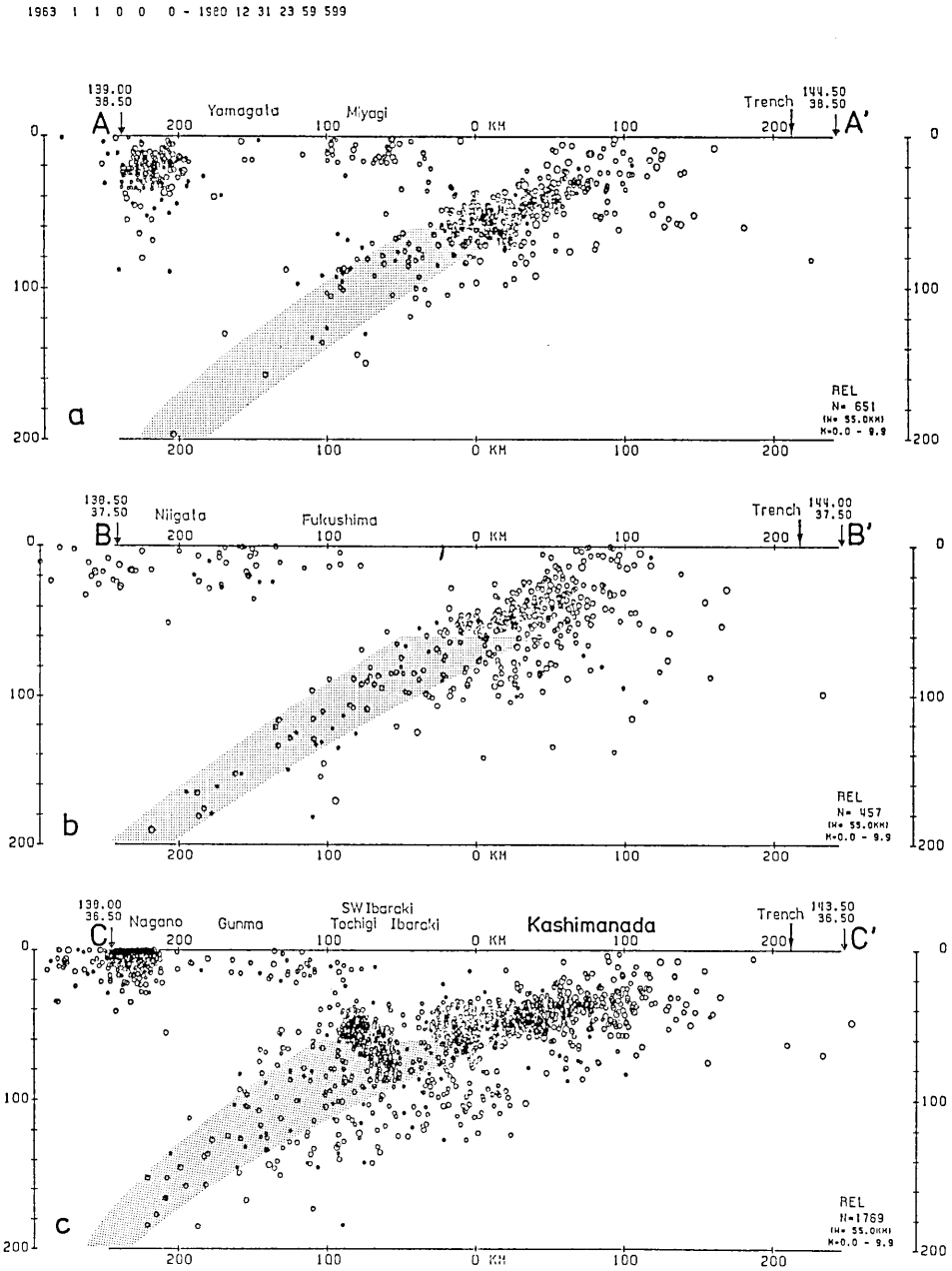

Fig. 6. a-c

southern sections (EE′ and FF′) an inclined pattern of seismic zones is not observed due to the small number of hypocenters, especially for that part deeper than 100 km. Some scattered hypocenters for the southern sections appear from the larger errors in hypocenter

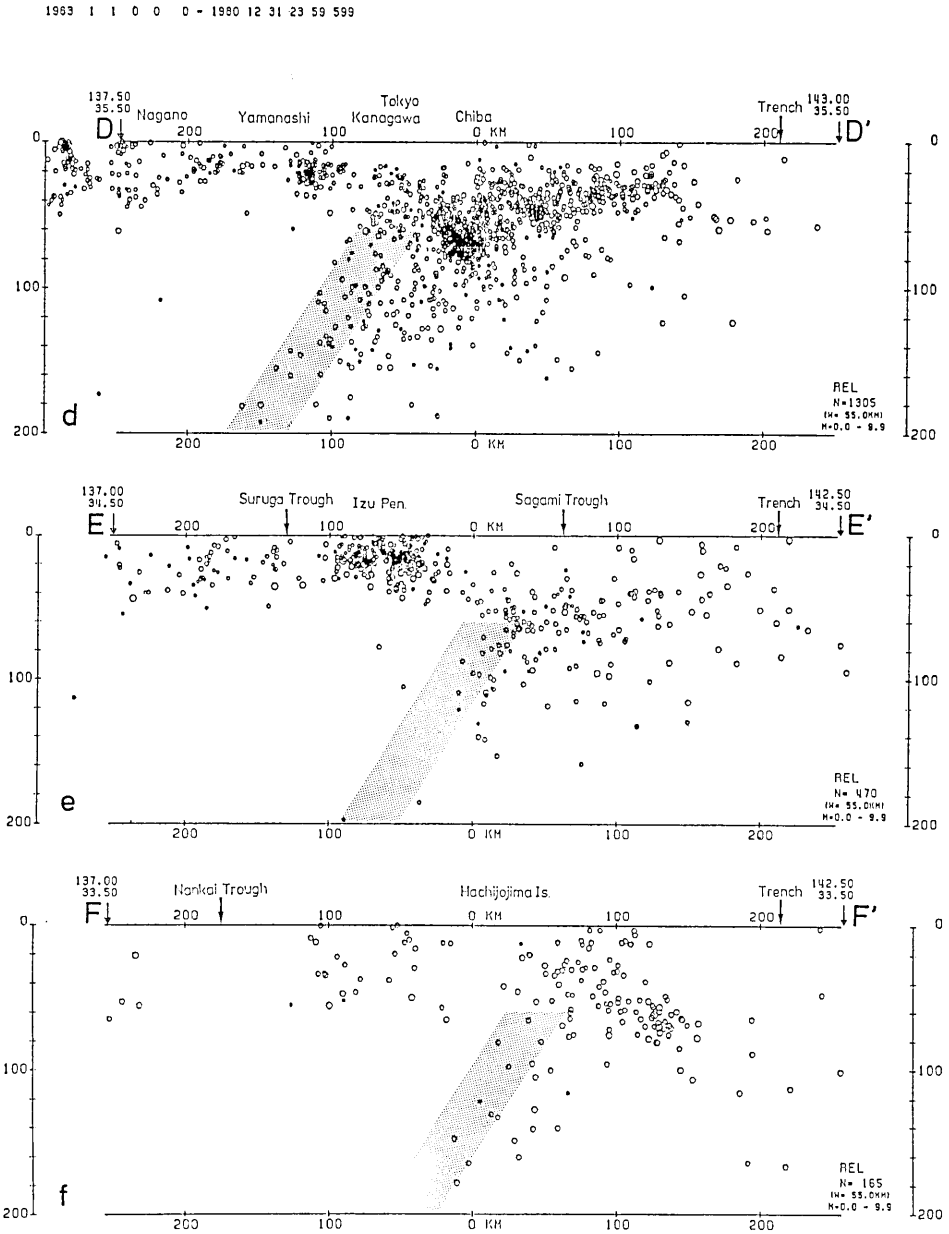

Fig. 6. Depth distributions of the relocated intermediate-depth earthquakes along the E-W sections of 110 km width between the following two points; (a) A (38.5°N, 139.0°E) and A′(38.5°N, 144.5°E), (b) B(37.5°N, 138.5°E) and B′(37.5°N, 144.0°E), (c) C(36.5°N, 138.0°E) and C′(36.5°N, 143.5°E), (d) D(35.5°N, 137.5°E) and D′(35.5°N, 143.0°E), (e) E(34.5°N, 137.0°E) and E′(34.5°N, 142.5°E) and (f) F(33.5°N, 137.0E) and F′(33.5°N, 142.5°E). Hatched areas denote possible ranges of the upper boundaries of the inclined seismic zone shown in Fig. 5.

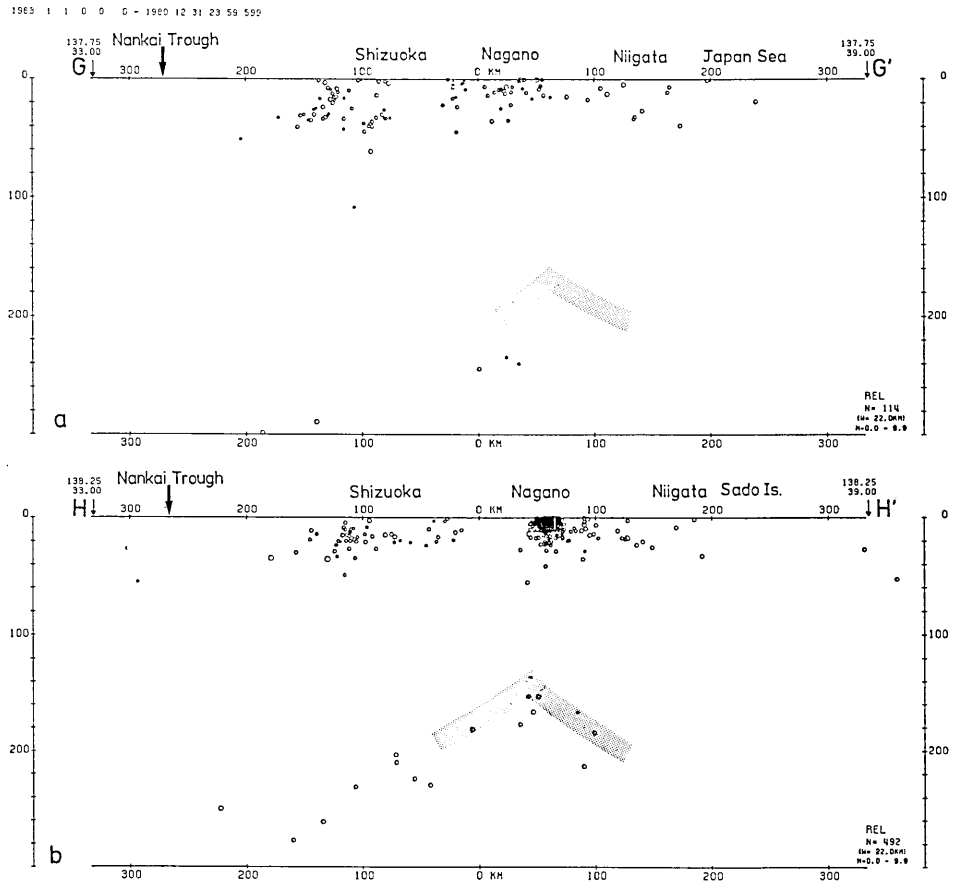

Fig. 7. a-b

locations due to the great distances from the stations (MAKI, 1982a).

Fig. 7 (GG′ to LL′) shows the depth distribution of relocated earthquakes along the N-S sections as shown in Fig. 5. Shaded areas denote positions of upper boundaries of the inclined seismic zone derived from the depth contours in Fig. 5. Earthquakes deeper than 200 km are also plotted for these sections. For the western sections (GG′, HH′, II′) an acute intersection of the Izu-Bonin slab dipping greater than the Northeast Honshu slab is observed. For the eastern sections (JJ′, KK′, LL′) the seismic zones are flattened. The intensely active region beneath the middle part of Chiba Prefecture is located within the intersecting region of the Northeast Honshu and Izu-Bonin slabs. Earthquakes beneath the southwestern end of Ibaraki Prefecture are located along the upper boundaries of the Northeast Honshu slab.

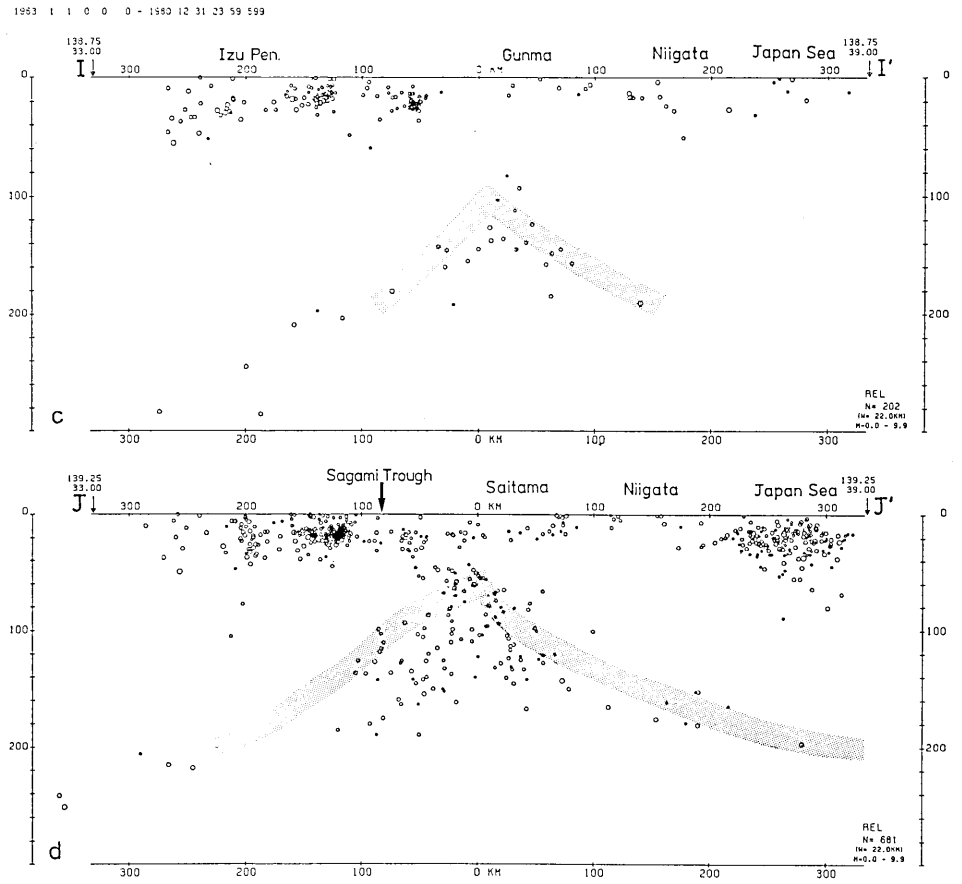

Fig. 7. c-d

Fig. 8 shows the comparison of depth distributions of hypocenters ($n=150$) which are located by the JMA routine (a), and (b) by the JHD (Joint Hypocenter Determination) method (MAKI, 1979). Even with the very wide section of 1°, the seismic zone from the precise location of hypocenters shows a space of 30 km between two parts. The relatively shallow hypocenters of the southern groups of the 36°N line suggest the upward convex plane of the Northeast Honshu slab.

The slab configuration was modeled from the spatial distribution of the relocated earthquakes by correcting the Pn station biases. The upper boundary of the inclined seismic zone was defined on the epicenter distributions of earthquakes for the depth interval of 20 km. These depth contours and depth distributions of hypocenters along the E-W and N-S sections suggest the acute intersection of the Northeast Honshu and Izu-Bonin slabs beneath the Kanto District. A gently

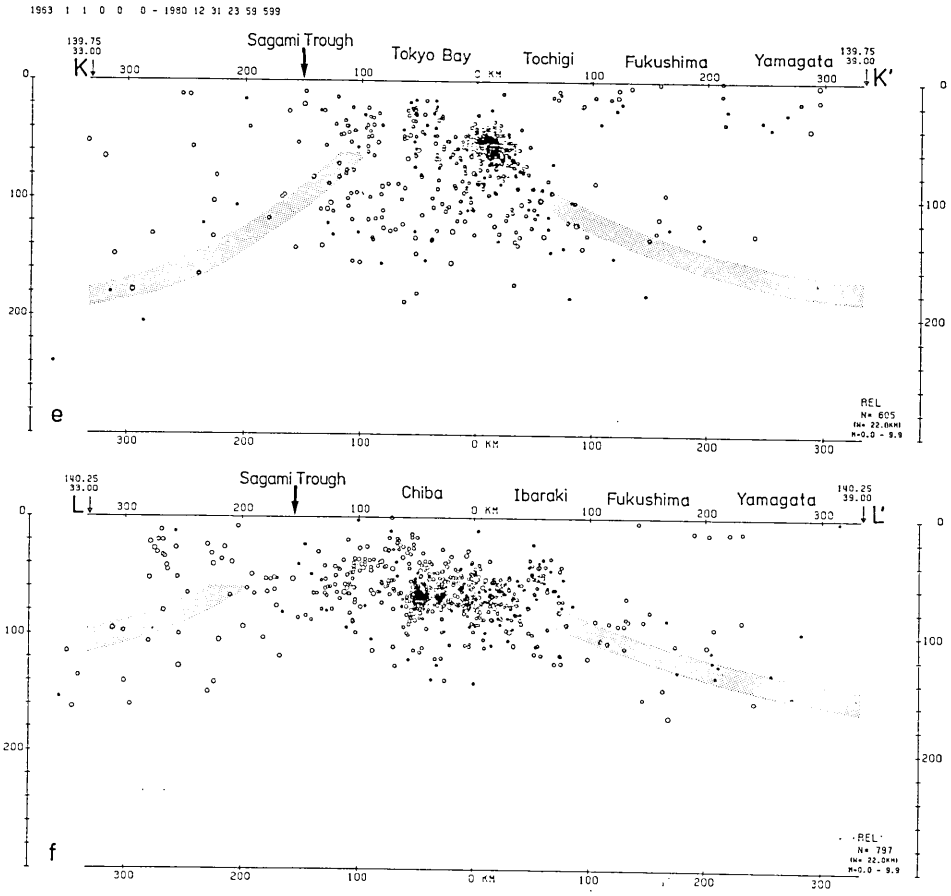

Fig. 7. Depth distributions of relocated intermediate-depth earthquakes along the N-S sections of the 44 km width between the following two points; (a) G(33.00°N, 137.75°E) and G'(39.00°N, 137.75°E), (b) H(33.00°N, 138.25°E) and H'(39.00°N, 138.25°E), (c) I(33.00°N, 138.75°E) and I'(39.00°N, 138.75°E), (d) J(33.00°N, 135.25°E) and J'(39.00°N, 139.25°E), (e) K(33.00°N, 139.75°E) and K'(39.00°N, 139.75°E) and (f) L(33.00°N, 140.25°E) and L'(39.00°N, 140.25°E).

dipping angle of about 30° is seen for the Northeast Honshu slab and a steeper angle of about 60° for the Izu-Bonin slab. The Northeast Honshu slab shows a strong northwestward bending at its shallower part. The double seismic planes were observed from other earthquakes located at the lower part or within the slab due to the small number of relocated earthquakes. For the sections south off the Kanto District such a double-layered structure is not seen.

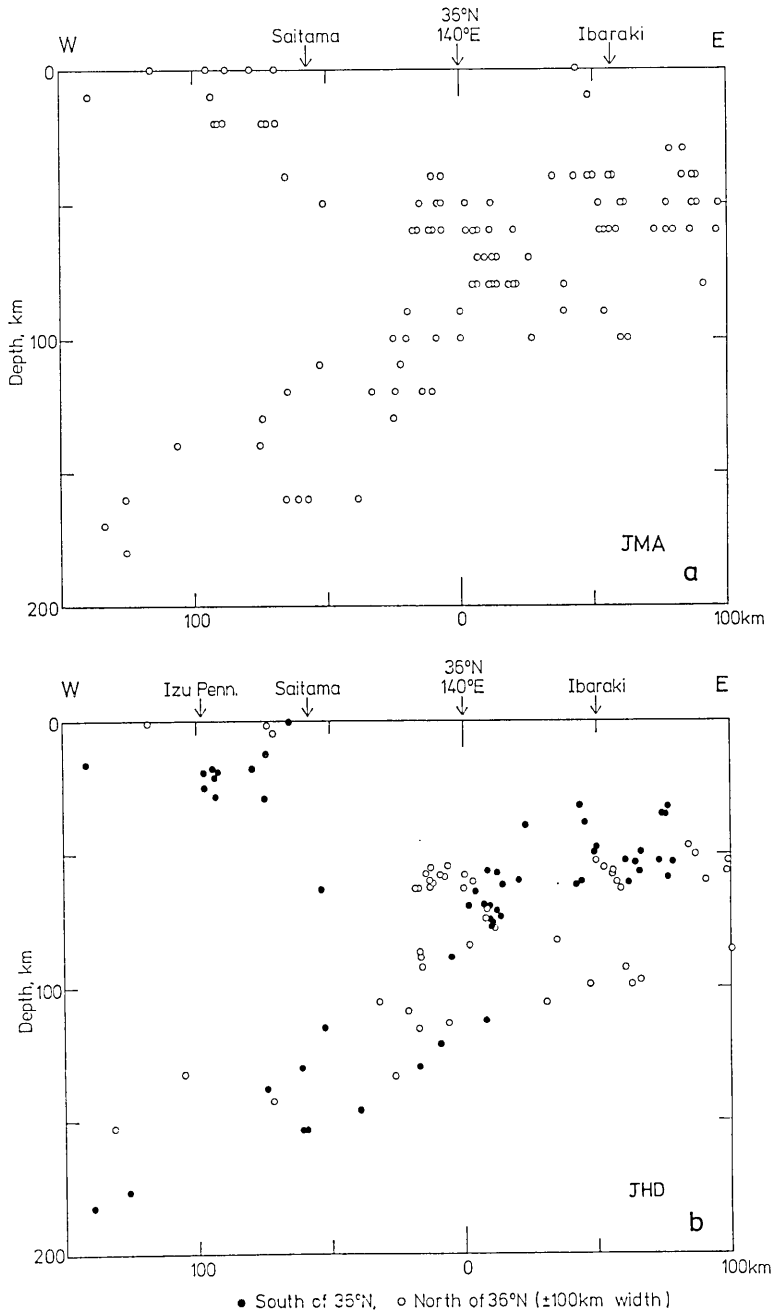

Fig. 8. Comparison of the depth distributions of intermediate-depth earthquakes along the E-W section of 100 km width around 36°N, (a) by the JMA routine and (b) by the Joint Hypocenter Determination (JHD) method (MAKI, 1979). Solid and empty circles in the lower part denote hypocenters which are located on the southern and northern sides of the latitude of 36°N.

3. Determination of fault-plane solutions of intermediate-depth earthquakes

Two types of focal mechanisms, the down-dip compression and extension along the upper and lower planes of the intermediate-depth seismic zone beneath Northeast Japan, have been identified from the fault-plane solutions for the composite first-motion data (UMINO and HASEGAWA, 1975, 1982; HASEGAWA *et al.*, 1978a). In Northeast Japan the down-dip stress is observed in the deeper half of the double seismic planes, but this pattern is disturbed in the shallower half. FUJITA and KANAMORI (1981) perferred the "in-plane" stresses to the "down-dip" stresses from the global survey of individual focal mechanisms. Focal mechanisms different from these two types are observed in the larger intermediate-depth earthquakes in the Kanto District (MAKI, 1983b). In the present chapter fault-plane solutions are determined for the greater number of earthquakes at intermediate-depths by the numerical method (MAKI, 1982b).

Fig. 9 shows a summary of the previous study of focal mechanisms for intermediate-depth earthquakes ($n=26$) which occurred at depths from 100 to 200 km with magnitudes of 5.0 or more during the period from 1963 to 1979 (MAKI, 1983b). For an intermediate-depth earthquake on September 25, 1972 (O.T.=18h25m53.4s, 142.43°E, 37.96°N, 115.7 km, M5.2), no first-motion data were reported. On the left-hand side (a) of Fig. 9 empty and solid circles denote axes of maximum

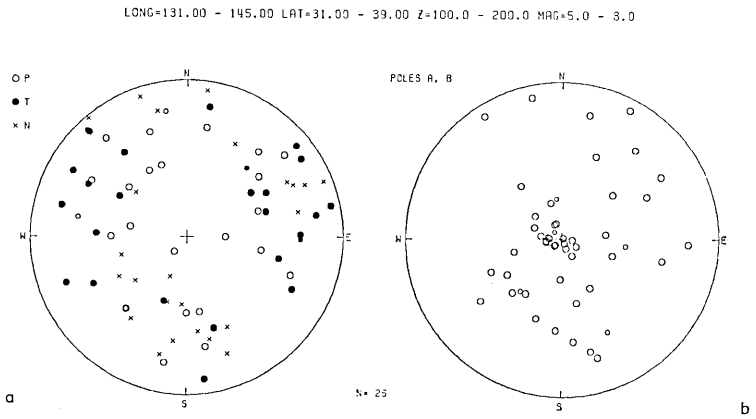

Fig. 9. Summary of fault-plane solutions of intermediate-depth earthquakes, which occurred at depths of $h=100\sim200$ km in and around the Kanto District with magnitudes of 5.0 or more during the period from 1963 to 1979 (MAKI, 1983b), by the equal-area projection of the lower focal hemisphere for P, T and N axes (a), and poles of nodal planes (b). Solid and empty circles and crosses denote axes of maximum tension and compression and null vector, respectively. Smaller symbols denote multiple solutions for same earthquakes.

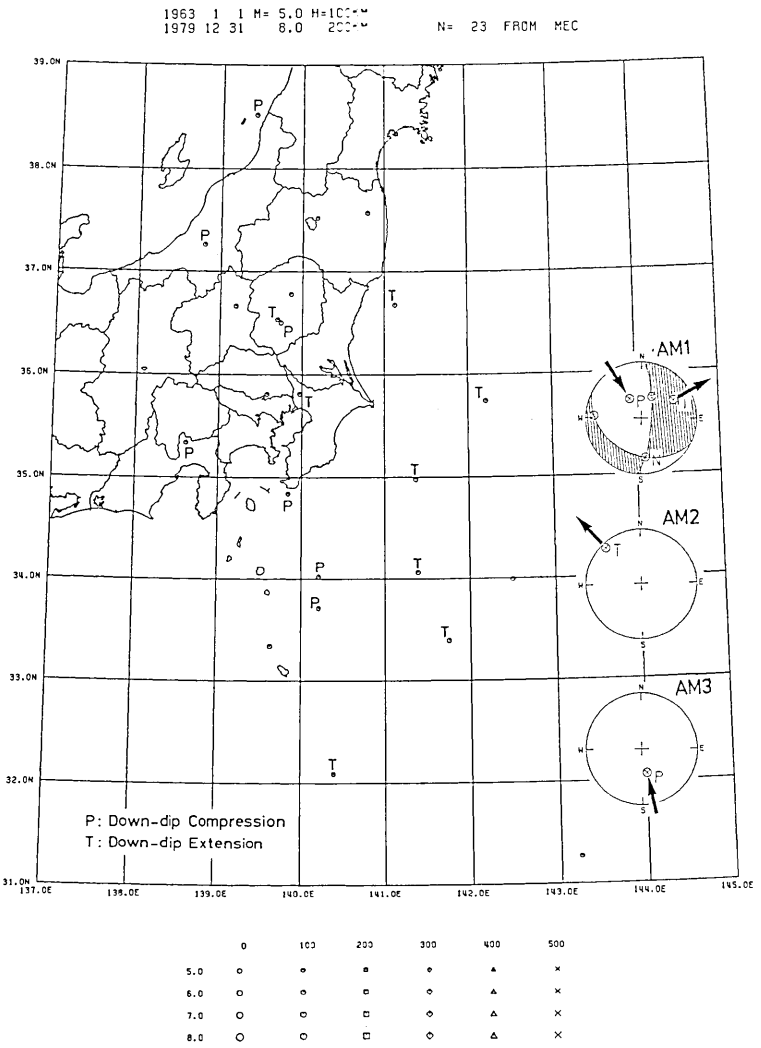

Fig. 10. Geographical distribution of mechanism types and average focal mechanisms of the intermediate-depth earthquakes (h=100~200 km, $M \geqq 5.0$) in and around the Kanto District during the period from 1963 to 1979 (MAKI, 1983b). Letters "P" and "T" beside epicenters denote the down-dip compression and extension, respectively. Three types of average focal mechanisms were obtained by the numerical averaging of direction cosines of P and T axes.

pressure (P) and tension (T), and crosses denote null vectors (N) for these solutions. Poles of nodal planes were shown by empty circles on the right-hand side (b). Three types of focal mechanisms are observed, namely (1) the down-dip compression to the northwest, (2) the extension dipping to the west, and (3) the compression or extension dipping to the south. Fig. 10 shows schematic diagrams of the aver-

age focal mechanisms (AM1 to 3) for these earthquakes and the distribution of epicenters classified by two types of focal mechanisms. Focal mechanisms with the down-dip compression along the inclined seismic zone ("P" beside epicenters) are observed in the inland region, and the down-dip extension ("T") on the Pacific side.

The fault-plane solutions have been obtained by the numerical method (MAKI, 1982b) for 42 intermediate-depth earthquakes which occurred at depths from 80 to 200 km with magnitudes of 5.0 or more during the period from 1963 to 1979. In the present study 12 fault-plane solutions are obtained for seven intermediate-depth earthquakes with magnitudes $M \geqq 5.0$ for the year of 1980, and 121 solutions for 95 earthquakes of magnitudes from 4.0 to 5.0 during the period from 1964 to 1980. First-motion data are also taken from BISC (Bulletin of the International Seismological Centre) and the JMA Monthly Seismological Bulletins. Take-off angles for the crust and upper mantle structure of the JMA standard travel-time table (ICHIKAWA and MOCHIZUKI, 1971) are calculated for each focal depth (MAKI, 1982b, 1983a). Multiple solutions are obtained for some earthquakes, but unique fault-plane solutions are determined for the majority of earthquakes. Scores of first-motion data are improved by an objective and automatic method of discarding the poor data based on station reliabilities for possible solutions of each earthquake. In the present study fault-plane solutions could be obtained for 144 out of 286 intermediate-depth earthquakes which occurred with magnitudes of 4 or more during the 18 years from 1963 to 1980. These solutions satisfy first-motion data of 10 or more.

Some types of fault-plane solutions and their first-motion data are shown in Figs. 11 to 14 by the equal-area projection of the lower focal hemisphere. A solution of the down-dip extension is uniquely determined for an intermediate-depth earthquake (M 5.5) which occurred off the Boso Peninsula at a depth of 92.2 km on October 28, 1979 (Fig. 11). On the left-hand side of the figure the confidence regions of fault-plane solutions with scores of 95% or more are shown for P, T and N axes. For this earthquake 157 first-motion data are given at first, but 30 first-motion data are automatically and objectively discarded based on station reliabilities for relatively possible solutions. On the right-hand side is shown the most suited fault-plane solution, which satisfies the remaining data, of the southwestern side sinking along the vertidal plane striking almost NW-SE. A solution of the down-dip compression is shown in Fig. 12 for an intermediate-depth earthquake which occurred beneath Shizuoka Prefecture on Nov. 6, 1976, at a depth of 180.7 km (M 5.1) with the confidence region of fault-plane solution on the upper part, and the first motion data on

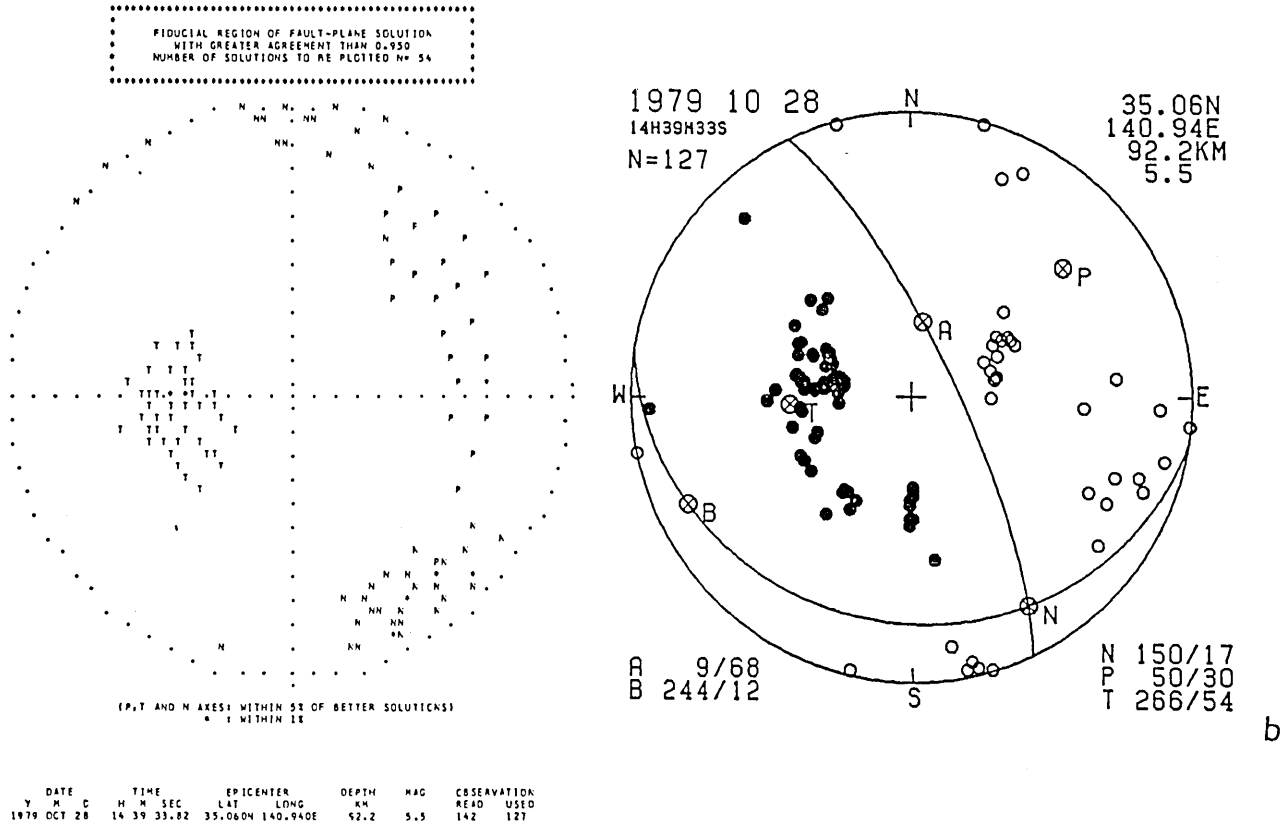

Fig. 11. Confidence region of fault-plane solution (a), and the most suited solution of focal mechanism with the down-dip extension (b) for an intermediate-depth earthquake which occurred off the Boso Peninsula on Oct. 28, 1979 (h=92.2 km, M5.5). Asterisks denote possible solutions with scores of 99% or more, and the letters "P", "T" and "N" denote less possible solutions for axes of maximum pressure and tension and null vector for scores from 95 to 99% (on the left-hand side). Solid and empty circles on the right denote compressional and dilatational first-motion data.

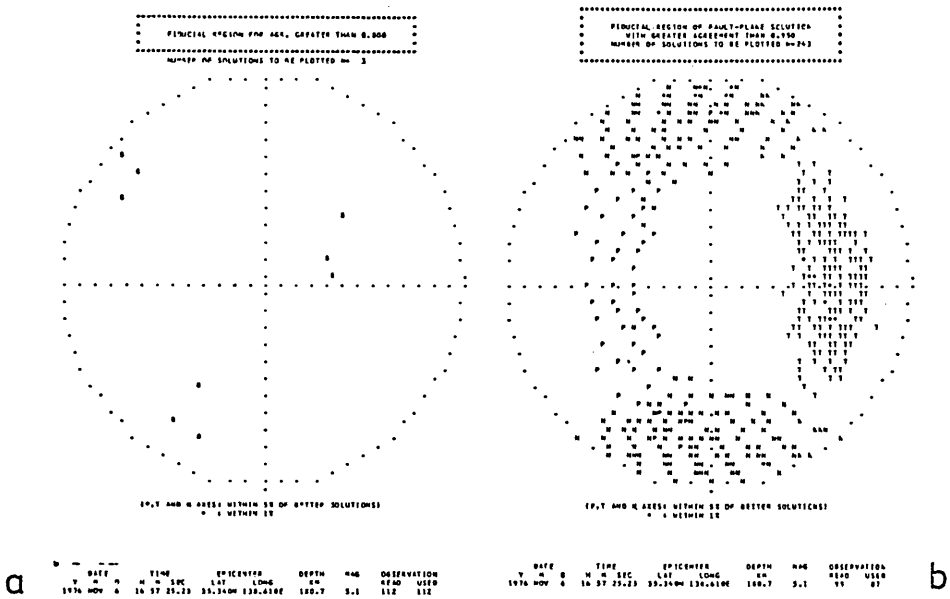

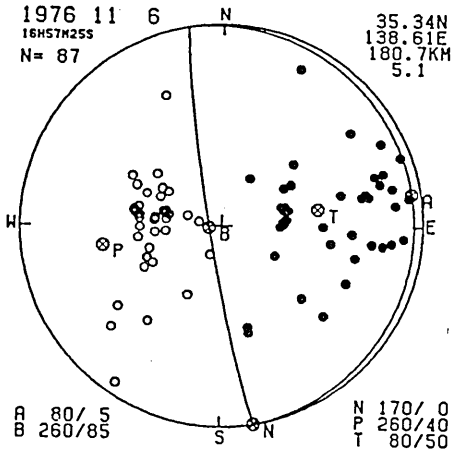

c

Fig. 12. Confidence regions of fault-plane solutions for all data of first motion (a), those with improved scores by discarding less-reliable first-motion data (b), and the most suited solution of focal mechanism with the down-dip compression toward the west (c), for an intermediate-depth earthquake which occurred beneath Shizuoka Prefecture on Nov. 6, 1976 (h=180.7 km, M5.1).

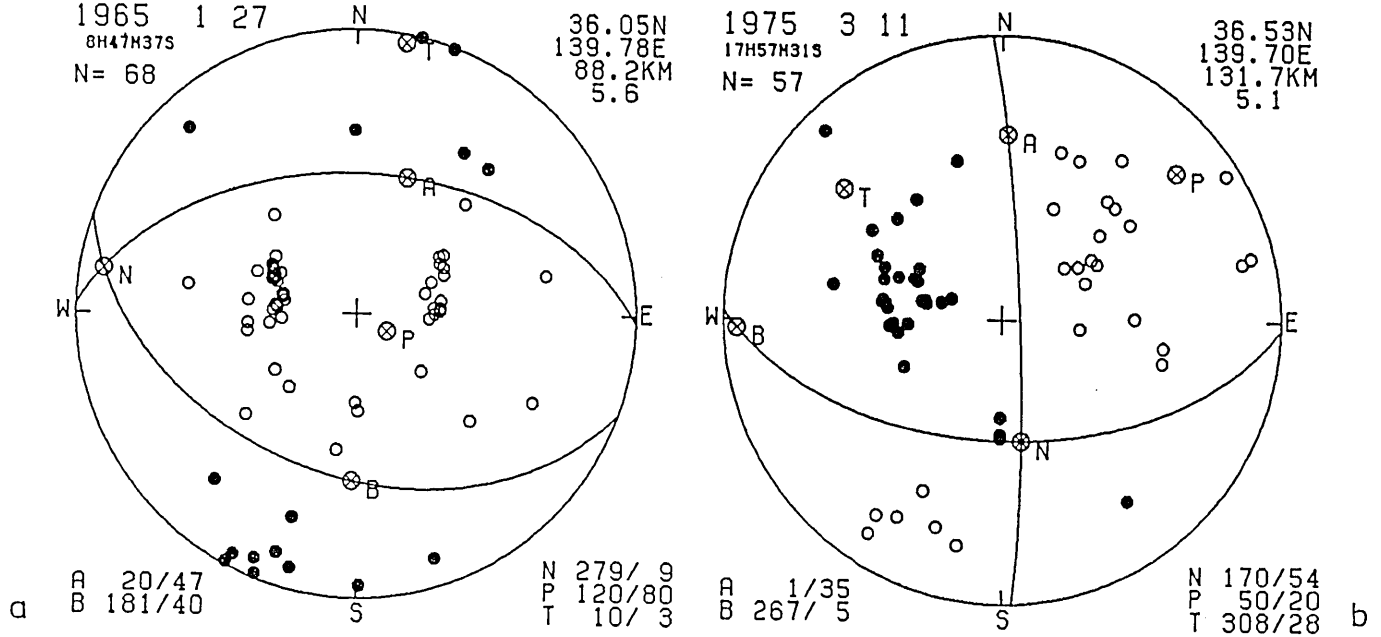

Fig. 13. (a) Normal fault with the N-S extension for an intermediate-depth earthquake which occurred beneath Ibaraki Prefecture on Jan. 27, 1965 (h=88.2 km, M5.6). (b) Strike-slip with the NW-SE extension for an intermediate-depth earthquake which occurred beneath Tochigi Prefecture on Mar. 11, 1975 (h=131.7 km, M5.1).

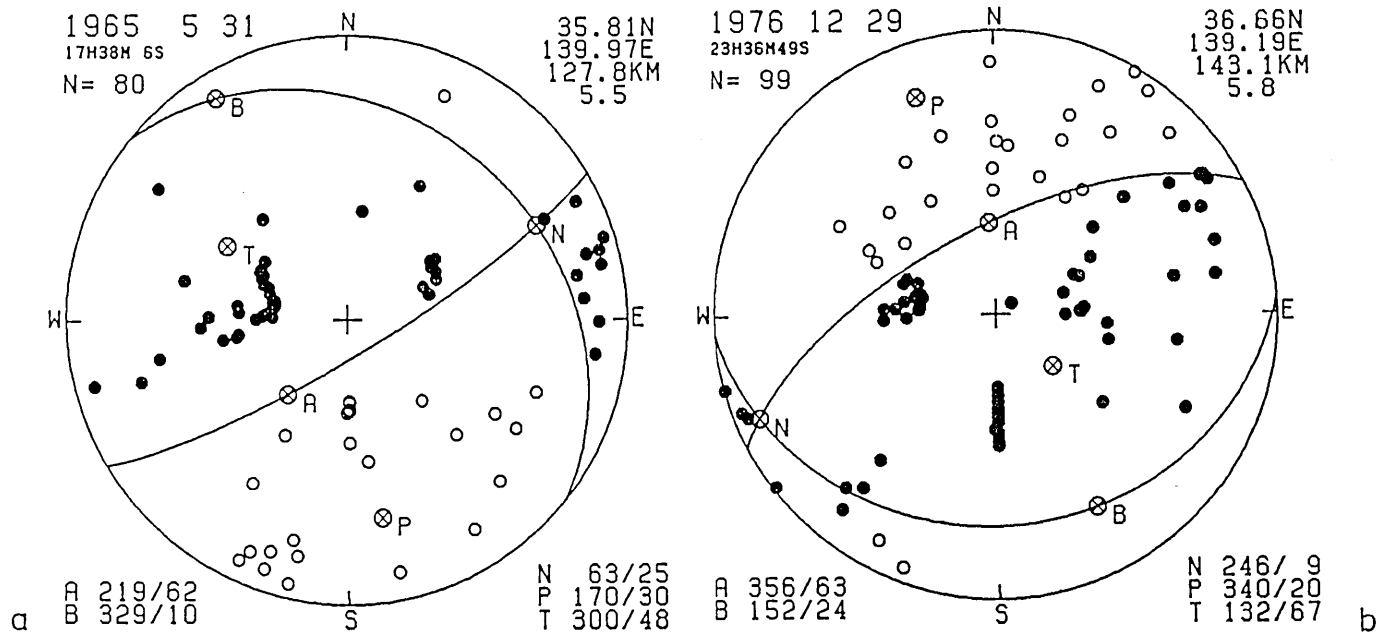

Fig. 14. (a) Hinge fault with the northern side downgoing along the nearly E-W striking nodal plane for an intermediate-depth earthquake which occurred beneath Chiba Prefecture on May 31, 1965 (h=127.8 km, M5.5). (b) Hinge fault with the southern side downgoing along the nearly E-W striking plane for an intermediate-depth earthquake which occurred beneath Gunma Prefecture on Dec. 29, 1976 (h=143.1 km, M5.8).

the lower part. Only low scores of about 80% were obtained as the first step for all the 112 first-motion data (a). After discarding 13 first-motion data based on station reliabilities for relatively possible solutions, many solutions with usable scores higher than 95% were obtained (b). The down-dip compression to the west is more probable in a sense of averaging. Fig. 13a shows another type of focal mechanism of the normal fault with an N-S extension for an intermediate-depth earthquake which occurred beneath the eastern part of Saitama Prefecture at a depth of 88.2 km on Jan. 27, 1965 (M 5.6). Fig. 13b shows a type of strike-slip with an NE-SW compression for an intermediate-depth earthquake which occurred beneath Gunma Prefecture at a depth of 131.7 km on March 11, 1975 (M 5.1). For this earthquake a thrust type of focal mechanism is also possible with the same score. Fig. 14 shows a hinge fault along the nearly vertical E-W nodal plane, (a) with the northern side sinking for an intermediate-depth earthquake which occurred beneath Chiba Prefecture on May 31, 1965 (h=127.8 km, M 5.5), and (b) with the southern side downgoing for an intermediate-depth earthquake which occurred beneath Gunma Prefecture on Dec. 29, 1976 (h=143.1 km, M 5.8).

Table 1 lists chronologically the fault-plane solutions (n=178) of 144 intermediate-depth earthquakes which occurred in and around the Kanto District during the period from 1963 to 1980 with magnitudes of 4.0 or more. Origin times and hypocenter locations are redetermined by correcting the JMA travel-time data with the Pn station biases (MAKI, 1982a), and the earthquake magnitudes are taken from JMA. "dd" and "d" mean dip direction and dip angle of poles and stress axes, and are given by the unit of tenth of a degree to keep the orthogonal relation within 1°. Numbers of first-motion data are shown for the read (all) and used ones (Nr and Nu) in the last two columns. The maximum difference of 0.4° from the orthogonal condition is observed for angular distances between the principal stresses and poles of nodal planes in the present study.

Fig. 15 shows the summary of fault-plane solutions for the intermediate-depth earthquakes with magnitudes of 5.0 or more in the upper part (n=57 solutions) and with magnitudes from 4.0 to 5.0 in the lower part (n=121). Empty and solid circles denote axes of maximum pressure (P) and tension (T), and null vectors (N) are denoted by crosses on the left-hand side. On the right-hand side poles of nodal planes are shown by empty circles. In comparison to relatively large earthquakes ($M \geqq 5.0$) variable types of focal mechanisms are observed for smaller earthquakes ($5 > M > 4$).

The variety of focal mechanisms suggests a complicated feature of earthquake-generating stress even at the intermediate-depth beneath

Table 1. Fault-plane solutions of intermediate-depth earthquakes which occurred at depths from 80 to 200 km in and around the Kanto District during the period from 1963 to 1980. "dd" and "d" mean dip direction and dip angle of axes of maximum pressure and tension and null vector, and poles of nodal planes. Origin times and focal coordinates of hypocenters are redetermined by correcting the JMA travel time data with the Pn station biases (MAKI, 1981a). Numbers of first-motion data are given in the last two columns for the read (all) and used ones.

No	Date y m d	Time h m s	Latit deg	Longit deg	Depth km	Mag	Pole-X dd	Pole-X d	Pole-Y dd	Pole-Y d	B-axis dd	B-axis d	P-axis dd	P-axis d	T-axis dd	T-axis d	Number all	Number used
1	63 221	14547	38.52	139.42	196.9	5.0	72.3	54.8	248.6	35.1	339.9	1.7	240.0	80.0	70.2	9.9	14 /	14
							14.6	48.4	107.2	2.3	199.2	41.6	320.0	30.0	72.8	33.8	14 /	14
2	63 221	113334	33.34	139.64	178.3	5.2	150.0	75.0	330.0	15.0	240.0	0.0	330.0	60.0	150.0	30.0	36 /	33
3	63 327	73647	34.02	140.21	105.0	5.0	34.3	62.0	261.1	20.0	164.0	18.8	290.0	60.0	65.9	22.5	15 /	13
							357.9	54.8	118.0	19.5	218.8	28.0	320.0	20.0	80.6	54.5	15 /	13
4	63 818	16 949	35.81	139.58	154.7	5.3	325.4	74.5	224.0	3.1	133.2	15.2	30.0	40.0	239.5	46.0	34 /	27
5	64 7 1	161632	35.27	139.95	89.8	4.5	268.0	54.0	108.5	34.3	11.8	9.9	280.0	10.0	145.4	75.9	15 /	15
6	64 7 3	153555	36.18	139.73	129.7	4.2	61.1	60.0	285.2	22.5	187.1	18.8	90.0	20.0	316.8	62.0	10 /	10
							166.1	63.7	322.3	24.4	56.6	9.4	150.0	20.0	302.7	67.7	10 /	10
7	64 726	182046	36.29	140.78	110.5	4.7	236.8	42.0	336.6	10.7	77.8	46.0	190.0	20.0	296.1	37.2	18 /	17
8	64 929	12554	34.06	141.39	106.5	5.0	12.2	54.8	252.0	19.5	151.2	28.0	50.0	20.0	289.4	54.5	23 /	22
							296.2	73.9	97.3	15.3	188.7	5.0	90.0	60.0	281.5	29.5	23 /	22
9	6411 3	11 540	34.83	140.78	97.5	5.2	177.3	32.8	62.7	32.8	300.0	40.0	120.0	50.0	210.0	0.0	41 /	35
10	641112	417 0	38.19	140.14	157.3	4.5	82.6	72.5	236.0	15.7	328.1	7.4	225.0	60.0	62.2	28.9	10 /	10
11	65 127	84737	36.05	139.78	88.2	5.6	20.2	47.6	181.5	40.9	279.7	9.4	120.0	80.0	10.3	3.4	79 /	68
12	65 128	03127	36.01	139.78	85.6	4.4	236.9	60.4	142.9	2.3	51.7	29.5	170.0	40.0	297.5	35.9	16 /	16
							103.1	60.4	197.1	2.3	288.3	29.5	170.0	40.0	42.6	35.9	16 /	16
13	65 222	72829	37.42	139.76	116.7	4.6	72.7	81.6	302.9	5.4	212.3	6.4	310.0	50.0	117.0	39.3	23 /	21
							145.8	57.1	275.9	22.7	15.9	22.5	240.0	60.0	114.0	18.8	23 /	21
							48.4	35.0	142.1	5.2	239.4	54.5	0.0	20.0	101.2	28.0	23 /	21
14	65 512	92819	37.72	139.13	181.1	4.5	196.9	55.4	97.2	6.6	2.8	33.8	250.0	30.0	129.2	41.6	11 /	10
							41.3	34.8	145.1	19.0	258.3	49.0	0.0	10.0	98.3	39.3	11 /	10
15	65 531	1738 6	35.81	139.97	127.8	5.5	219.1	62.1	329.0	10.2	63.9	25.7	170.0	30.0	300.9	48.6	87 /	80
16	65 614	232818	35.59	139.30	154.7	4.7	261.1	56.5	14.0	14.5	112.4	29.5	340.0	50.0	217.3	24.4	14 /	14
17	65 7 4	024 9	35.21	140.08	113.7	4.8	144.6	7.1	235.4	7.1	10.0	80.0	190.0	10.0	100.0	0.0	33 /	26
18	65 728	145833	36.10	138.74	137.7	4.4	122.6	38.4	8.2	27.6	253.0	39.3	60.0	50.0	157.7	6.4	16 /	16
19	65 914	18 039	34.98	141.37	115.6	5.3	317.3	75.7	74.1	6.6	165.6	12.7	60.0	50.0	265.4	37.2	17 /	15
20	651014	043 9	36.35	139.63	104.6	4.6	67.5	27.0	172.6	27.0	300.0	50.0	30.0	0.0	120.0	40.0	31 /	25
21	651023	233028	35.54	140.18	81.5	4.6	155.3	53.4	57.0	6.1	322.6	35.9	90.0	40.0	208.3	29.5	19 /	18
							27.2	46.5	128.5	10.6	228.1	41.6	90.0	40.0	339.6	22.5	19 /	18
22	66 429	1125 4	36.67	140.26	80.5	4.7	286.1	63.7	82.3	24.4	176.6	9.4	270.0	20.0	62.7	67.7	29 /	25
23	66 6 2	21 754	36.18	139.42	128.2	4.4	80.8	68.3	205.6	12.8	299.7	17.2	40.0	30.0	184.0	54.5	14 /	12
24	66 623	143919	38.17	139.83	130.1	4.3	32.7	81.6	262.9	5.4	172.3	6.4	270.0	50.0	77.0	39.3	15 /	14
							125.4	41.3	217.8	2.7	310.9	48.6	180.0	30.0	73.9	25.7	15 /	14
25	66 624	65156	38.08	141.68	83.6	5.1	325.0	62.9	77.6	11.2	172.7	24.4	50.0	50.0	277.6	29.5	36 /	36
26	66 918	93518	37.06	140.88	97.9	4.8	257.0	41.0	10.1	24.3	121.7	39.3	220.0	10.0	321.7	49.0	14 /	13
27	661218	34548	37.24	141.40	87.1	4.7	164.3	62.0	31.1	20.0	294.0	18.8	60.0	60.0	195.9	22.5	12 /	12

Table 1. (Continued)

No	Date y m d	Time h m s	Latit deg	Longit deg	Depth km	Mag	Pole-X dd	d	Pole-Y dd	d	B-axis dd	d	P-axis dd	d	T-axis dd	d	Number all	used
28	67 319	24948	36.28	140.05	97.3	5.5	183.5	34.3	87.8	8.3	346.1	54.5	130.0	30.0	230.3	17.2	71 /	61
29	67 7 9	41820	37.77	143.88	98.8	5.1	79.9	44.1	240.2	44.1	340.0	10.0	70.0	0.0	160.0	80.0	20 /	20
30	67 812	133040	38.31	142.15	83.4	5.4	290.2	44.1	129.9	44.1	30.0	10.0	210.0	80.0	300.0	0.0	70 /	66
31	67 819	223817	36.31	140.33	108.9	4.6	356.0	28.1	258.9	13.0	146.7	58.5	40.0	10.0	304.3	29.5	33 /	29
							300.0	75.0	120.0	15.0	30.0	0.0	120.0	60.0	300.0	30.0	33 /	29
32	6710 3	55338	35.06	139.32	136.9	4.4	239.2	68.3	114.4	12.8	20.3	17.2	280.0	30.0	136.1	54.5	11 /	10
33	671017	22642	36.09	138.80	126.6	4.7	122.6	27.0	17.5	27.0	250.0	50.0	70.0	40.0	160.0	0.0	18 /	17
							317.7	54.8	141.4	35.1	50.2	1.7	150.0	80.0	319.9	9.9	18 /	17
34	68 121	1326 5	33.35	142.03	100.0	4.7	296.6	37.8	63.4	37.8	180.0	30.0	0.0	60.0	270.0	0.0	17 /	13
35	68 529	19 350	36.14	140.40	87.1	4.9	241.8	20.9	334.6	7.3	82.7	67.7	290.0	20.0	196.6	9.4	30 /	24
36	68 7 4	93412	34.84	139.84	109.2	5.2	22.4	69.3	269.1	8.5	176.1	18.8	290.0	50.0	73.0	33.8	65 /	57
37	68 9 3	16 135	37.90	141.94	88.2	5.4	348.4	27.4	85.9	14.3	200.6	58.5	40.0	30.0	305.0	8.7	56 /	55
38	69 217	1629 7	37.50	140.96	107.0	4.9	59.9	44.1	220.2	44.1	320.0	10.0	50.0	0.0	140.0	80.0	33 /	29
39	69 4 9	215724	36.78	139.86	122.0	5.6	181.6	35.0	87.9	5.2	350.6	54.5	230.0	20.0	128.8	28.0	127 /	117
40	69 620	1541 4	38.44	142.22	92.0	5.6	143.5	34.3	47.8	8.3	306.1	54.5	90.0	30.0	190.3	17.2	56 /	54
41	69 627	234242	35.91	139.51	94.7	4.4	96.1	63.7	252.3	24.4	346.6	9.4	80.0	20.0	232.7	67.7	15 /	12
42	69 8 6	33432	37.57	140.80	124.7	5.0	233.3	60.9	76.6	27.1	341.5	9.9	100.0	70.0	248.4	17.2	41 /	37
43	69 911	152039	38.21	141.76	96.3	4.7	97.3	30.8	194.1	11.3	301.8	56.8	150.0	30.0	52.4	13.0	11 /	11
44	691030	9 539	37.52	140.18	170.6	5.5	50.0	55.0	230.0	35.0	140.0	0.0	230.0	80.0	50.0	10.0	63 /	63
45	691130	214854	34.73	139.95	81.7	4.5	70.0	45.0	250.0	45.0	340.0	0.0	70.0	0.0	250.0	90.0	14 /	12
							160.0	45.0	340.0	45.0	70.0	0.0	160.0	0.0	340.0	90.0	14 /	12
46	691229	243 5	35.53	139.80	133.4	4.5	188.2	20.9	95.4	7.3	347.3	67.7	140.0	20.0	233.5	9.4	14 /	13
47	70 412	175417	38.81	140.90	149.5	4.9	267.3	75.7	24.1	6.6	115.6	12.7	10.0	50.0	215.4	37.2	45 /	39
48	70 517	235150	34.64	141.23	88.1	5.2	59.1	20.7	320.9	20.7	190.0	60.0	100.0	0.0	10.0	30.0	56 /	53
49	70 626	123529	32.09	140.39	186.7	5.0	26.4	33.3	281.7	21.1	165.3	49.0	330.0	40.0	66.5	7.6	14 /	14
50	70 720	133623	35.59	140.20	81.9	4.4	358.4	35.0	92.1	5.2	189.4	54.5	310.0	20.0	51.2	28.0	19 /	18
51	70 818	6 238	36.25	140.43	96.2	4.1	335.5	54.3	162.7	35.5	70.3	3.4	180.0	80.0	339.7	9.4	11 /	11
52	71 128	215742	35.20	139.40	127.0	4.5	321.7	27.4	224.1	14.3	109.4	58.5	270.0	30.0	5.0	8.7	22 /	20
53	71 129	1535 6	36.04	139.79	87.8	4.5	119.0	60.0	254.8	22.5	352.9	18.8	90.0	20.0	223.2	62.0	17 /	16
54	71 312	510 9	35.49	139.14	135.4	4.5	268.4	27.4	5.9	14.3	120.6	58.5	320.0	30.0	225.0	8.7	21 /	19
55	71 424	84659	36.38	139.04	167.3	4.4	349.1	20.7	250.9	20.7	120.0	60.0	30.0	0.0	300.0	30.0	14 /	12
							142.0	54.0	301.5	34.3	38.3	9.9	130.0	10.0	264.6	75.9	14 /	12
56	71 425	201753	35.59	140.11	81.7	4.1	183.8	73.9	22.7	15.3	291.3	5.0	30.0	60.0	198.5	29.5	14 /	12
57	71 614	191729	37.87	140.52	94.2	4.2	211.1	41.6	68.9	41.6	320.0	20.0	230.0	0.0	140.0	70.0	10 /	10
58	71 921	174332	37.26	138.80	190.6	5.7	49.7	45.0	267.2	38.5	160.6	19.7	330.0	70.0	69.4	3.4	126 /	115

Table 1. (Continued)

No	Date	Time	Latit	Longit	Depth	Mag	Pole-X		Pole-Y		B-axis		P-axis		T-axis		Number	
	y m d	h m s	deg	deg	km		dd	d	dd	d	dd	d	dd	d	dd	d	all	used
59	711121	14715	31.53	142.81	120.5	4.8	173.0	41.0	59.9	24.3	308.3	39.3	210.0	10.0	108.3	49.0	11 /	11
60	72 3 1	182531	33.20	141.31	99.8	5.1	306.8	42.0	46.5	10.7	147.8	46.0	260.0	20.0	6.0	37.2	15 /	14
61	72 314	161536	35.57	139.96	81.0	4.4	138.8	28.0	48.4	0.8	316.8	62.0	90.0	20.0	187.1	18.8	11 /	11
							241.1	55.1	29.0	30.6	128.2	15.2	350.0	70.0	221.7	12.7	11 /	11
62	72 331	44242	33.94	140.06	149.1	4.5	149.1	46.5	23.8	28.7	275.7	29.5	180.0	10.0	73.3	58.5	17 /	15
							134.6	21.2	42.0	6.6	295.5	67.7	180.0	10.0	86.4	19.7	17 /	15
63	72 518	34512	37.81	140.42	109.2	4.7	26.7	60.9	183.4	27.1	278.5	9.9	160.0	70.0	11.6	17.2	29 /	26
64	72 613	18 141	36.31	138.99	93.1	4.3	326.5	34.3	62.2	8.3	164.0	54.5	20.0	30.0	279.7	17.2	14 /	12
							83.4	37.8	316.6	37.8	200.0	30.0	20.0	60.0	110.0	0.0	14 /	12
65	72 810	112744	35.58	139.24	106.0	4.3	151.7	27.4	54.1	14.3	299.4	58.5	100.0	30.0	195.0	8.7	11 /	11
66	72 926	1 031	35.95	138.44	181.3	4.8	15.4	7.1	284.6	7.1	150.0	80.0	330.0	10.0	60.0	0.0	46 /	42
67	721029	25415	33.20	140.21	95.6	5.0	86.1	63.7	242.3	24.4	336.6	9.4	70.0	20.0	222.7	67.7	25 /	21
							38.4	27.4	135.9	14.3	250.6	58.5	90.0	30.0	355.0	8.7	25 /	21
68	721119	755 9	37.35	139.75	133.9	4.4	53.8	73.9	252.7	15.3	161.3	5.0	260.0	60.0	68.5	29.5	19 /	18
69	7212 5	23 334	33.39	141.75	115.6	5.3	285.0	75.0	105.0	15.0	15.0	0.0	105.0	60.0	285.0	30.0	30 /	30
							346.0	10.6	254.0	10.6	120.0	75.0	30.0	0.0	300.0	15.0	30 /	30
70	7212 7	95420	33.01	141.17	96.9	4.6	307.5	27.0	52.6	27.0	180.0	50.0	270.0	0.0	0.0	40.0	19 /	16
71	7212 8	13 339	31.27	143.23	124.4	5.0	56.5	34.3	152.2	8.3	254.0	54.5	110.0	30.0	9.7	17.2	11 /	11
72	721223	23532	33.20	139.63	147.8	4.6	165.0	60.0	345.0	30.0	75.0	0.0	165.0	15.0	345.0	75.0	10 /	10
73	73 415	83723	34.48	139.88	98.8	4.4	272.6	51.0	53.4	32.1	156.4	19.7	250.0	10.0	5.5	67.7	17 /	15
74	73 824	41642	36.50	139.74	101.2	5.0	16.9	60.4	282.9	2.3	191.7	29.5	310.0	40.0	77.5	35.9	59 /	47
75	731221	55315	33.98	140.19	141.1	4.8	329.1	20.7	230.9	20.7	100.0	60.0	10.0	0.0	280.0	30.0	33 /	26
							277.7	63.1	114.4	25.9	21.1	6.7	130.0	70.0	288.8	18.8	33 /	26
76	74 2 7	213337	37.36	141.26	82.5	4.6	112.4	69.3	359.1	8.5	266.1	18.8	20.0	50.0	163.0	33.8	21 /	18
77	74 4 4	1637 3	37.63	140.89	99.9	5.2	53.4	37.8	286.6	37.8	170.0	30.0	80.0	0.0	350.0	60.0	76 /	71
78	74 420	31852	35.24	139.44	118.6	4.3	92.7	81.6	322.9	5.4	232.3	6.4	330.0	50.0	137.0	39.3	14 /	14
79	74 7 3	41944	37.71	141.78	80.8	4.8	20.0	65.0	200.0	25.0	110.0	0.0	200.0	70.0	20.0	20.0	25 /	21
							335.4	21.2	68.0	6.6	174.5	67.7	290.0	10.0	23.6	19.7	25 /	21
80	74 715	02452	33.34	140.11	160.5	4.8	112.0	54.0	271.5	34.3	8.3	9.9	100.0	10.0	234.6	75.9	21 /	16
81	7411 4	102615	36.58	140.54	103.2	4.2	295.9	57.3	99.5	31.6	194.2	7.4	75.0	75.0	285.9	13.0	13 /	12
82	75 121	175629	33.38	141.14	80.7	4.9	142.5	70.8	355.4	16.3	262.5	9.9	10.0	60.0	167.2	28.0	21 /	18
							206.8	14.0	113.2	14.0	340.0	70.0	250.0	0.0	160.0	20.0	21 /	18
83	75 3 4	02923	34.49	140.32	118.7	4.5	223.7	58.6	119.6	8.4	24.7	30.0	150.0	45.0	275.3	30.0	16 /	15
84	75 311	175731	36.53	139.70	131.7	5.1	1.6	35.0	267.9	5.2	170.6	54.5	50.0	20.0	308.8	28.0	62 /	57
85	75 426	23733	37.89	141.38	93.1	5.0	317.7	63.1	154.4	25.9	61.1	6.7	170.0	70.0	328.8	18.8	46 /	42

Table 1. (Continued)

No	Date y m d	Time h m s	Latit deg	Longit deg	Depth km	Mag	Pole-X dd	Pole-X d	Pole-Y dd	Pole-Y d	B-axis dd	B-axis d	P-axis dd	P-axis d	T-axis dd	T-axis d	Number all	Number used
86	75 716	7 214	36.47	140.38	116.1	4.2	160.0	25.0	340.0	65.0	70.0	0.0	160.0	70.0	340.0	20.0	11 /	10
							161.7	27.4	64.1	14.3	309.4	58.5	110.0	30.0	205.0	8.7	11 /	10
87	76 2 7	33846	36.29	138.55	145.2	4.5	265.1	73.1	117.3	14.5	25.0	8.7	290.0	30.0	129.4	58.5	21 /	19
88	76 222	101224	36.35	140.70	102.9	4.9	145.1	73.1	357.3	14.5	265.0	8.7	170.0	30.0	9.4	58.5	61 /	49
89	76 225	237 0	37.21	141.06	99.7	5.0	23.0	41.0	269.9	24.3	158.3	39.3	60.0	10.0	318.3	49.0	61 /	54
90	76 227	15133	38.15	140.85	143.9	4.6	56.4	33.3	311.7	21.1	195.3	49.0	0.0	40.0	96.5	7.6	39 /	32
							289.8	49.3	92.4	39.4	189.6	8.7	40.0	80.0	280.4	5.0	39 /	32
91	76 328	151910	37.26	141.18	80.8	4.4	68.2	20.9	335.4	7.3	227.3	67.7	20.0	20.0	113.5	9.4	13 /	12
							156.6	37.8	283.4	37.8	40.0	30.0	220.0	60.0	130.0	0.0	13 /	12
92	76 524	202430	31.62	141.98	86.7	5.7	349.2	68.3	224.4	12.8	130.3	17.2	30.0	30.0	246.1	54.5	95 /	87
							176.9	60.4	82.9	2.3	351.7	29.5	110.0	40.0	237.5	35.9	95 /	87
93	76 718	17 732	36.03	139.78	85.3	4.4	119.0	60.0	254.8	22.5	352.9	18.8	90.0	20.0	223.2	62.0	24 /	24
94	76 823	15 1 0	35.78	139.92	106.8	4.1	345.4	7.1	254.6	7.1	120.0	80.0	30.0	0.0	300.0	10.0	18 /	16
95	7610 6	223841	37.07	141.44	91.2	5.9	273.8	73.9	112.7	15.3	21.3	5.0	120.0	60.0	288.5	29.5	178 /	157
							218.4	35.0	312.1	5.2	49.4	54.5	170.0	20.0	271.2	28.0	178 /	157
96	761030	94354	34.80	139.79	140.3	4.6	150.0	85.0	330.0	5.0	60.0	0.0	150.0	40.0	330.0	50.0	51 /	42
97	7611 6	165725	35.34	138.61	180.7	5.1	80.0	5.0	260.0	85.0	170.0	0.0	260.0	40.0	80.0	50.0	99 /	87
98	761213	115559	36.74	140.70	103.3	4.6	175.5	54.3	2.7	35.5	270.3	3.4	20.0	80.0	179.7	9.4	24 /	22
99	761229	233649	36.66	139.19	143.1	5.8	356.1	63.7	152.3	24.4	246.6	9.4	340.0	20.0	132.7	67.7	103 /	99
100	77 5 8	13 128	35.39	139.07	159.5	4.3	154.0	50.8	277.2	24.1	21.5	28.9	120.0	15.0	234.2	56.8	15 /	13
101	77 6 8	232545	38.46	141.79	82.3	5.8	72.6	27.0	327.5	27.0	200.0	50.0	110.0	0.0	20.0	40.0	155 /	125
102	77 830	233331	33.52	141.30	84.8	4.2	150.0	60.0	330.0	30.0	60.0	0.0	150.0	15.0	330.0	75.0	13 /	10
103	77 9 6	1110 6	36.83	139.96	142.0	4.0	37.3	81.6	167.1	5.4	257.7	6.4	160.0	50.0	353.0	39.3	17 /	15
							304.0	28.1	41.1	13.0	153.3	58.5	260.0	10.0	355.7	29.5	17 /	15
104	771116	235838	36.10	140.52	104.0	4.6	187.3	67.5	279.3	0.8	9.6	22.5	120.0	40.0	258.1	41.6	33 /	27
105	771118	22032	33.71	140.21	127.4	5.7	330.8	68.3	95.6	12.8	189.7	17.2	290.0	30.0	74.0	54.5	155 /	134
106	771227	1851 7	35.16	139.63	118.0	4.0	153.4	37.8	26.6	37.8	270.0	30.0	180.0	0.0	90.0	60.0	18 /	14
107	78 121	7 031	36.87	140.90	80.9	4.1	177.7	63.1	14.4	25.9	281.1	6.7	30.0	70.0	188.8	18.8	13 /	12
							127.9	54.8	248.0	19.5	348.8	28.0	90.0	20.0	210.6	54.5	13 /	12
108	78 121	111736	36.34	140.61	90.7	4.4	166.7	50.3	280.2	18.3	23.0	33.8	240.0	50.0	126.1	18.8	23 /	21
109	78 324	65158	37.63	141.73	84.2	4.2	104.0	10.6	196.0	10.6	330.0	75.0	60.0	0.0	150.0	15.0	18 /	17
110	78 615	21347	36.74	140.92	96.5	4.2	97.8	48.6	350.8	14.5	249.2	37.8	30.0	45.0	142.2	20.7	15 /	14
111	78 715	191841	33.41	141.85	88.7	4.9	30.0	45.0	210.0	45.0	300.0	0.0	30.0	0.0	210.0	90.0	39 /	39
							300.0	45.0	120.0	45.0	30.0	0.0	120.0	0.0	300.0	90.0	39 /	39
112	78 731	95038	36.57	138.97	148.6	4.2	82.7	81.6	312.9	5.4	222.3	6.4	320.0	50.0	127.0	39.3	18 /	15

Table 1. (Continued)

No	Date y m d	Time h m s	Latit deg	Longit deg	Depth km	Mag	Pole-X dd	d	Pole-Y dd	d	B-axis dd	d	P-axis dd	d	T-axis dd	d	Number all	used
113	78 815	215516	33.99	142.50	101.1	5.0	300.0	30.0	120.0	60.0	210.0	0.0	300.0	75.0	120.0	15.0	26 /	26
114	78 9 7	22 430	38.01	141.17	92.6	4.7	307.9	54.8	68.0	19.5	168.8	28.0	270.0	20.0	30.6	54.5	30 /	24
115	78 9 9	205944	37.04	141.45	90.7	4.5	122.1	21.1	31.9	0.4	301.0	68.9	75.0	15.0	169.0	14.5	15 /	15
116	78 914	214526	33.57	140.76	95.9	4.6	75.0	0.0	345.0	0.0	210.0	90.0	30.0	0.0	120.0	0.0	11 /	10
117	78 919	54428	34.21	140.21	93.6	5.0	343.4	37.8	216.6	37.8	100.0	30.0	280.0	60.0	10.0	0.0	35 /	30
118	78 920	25323	36.89	140.35	119.7	4.2	293.3	60.9	136.6	27.1	41.5	9.9	160.0	70.0	308.4	17.2	14 /	13
119	781011	104859	33.47	141.13	80.4	5.7	130.0	45.0	310.0	45.0	40.0	0.0	130.0	0.0	310.0	90.0	187 /	181
120	781020	85814	35.96	139.28	99.2	4.2	220.0	85.0	40.0	5.0	310.0	0.0	40.0	50.0	220.0	40.0	17 /	15
121	781228	1 6 6	35.81	139.49	99.2	4.2	48.4	27.4	145.9	14.3	260.6	58.5	100.0	30.0	5.0	8.7	19 /	18
122	79 1 1	1239 6	35.75	138.90	146.1	4.0	53.4	64.5	242.2	25.2	150.6	3.4	250.0	70.0	59.4	19.7	14 /	12
123	79 1 8	172717	37.05	140.93	100.9	4.1	194.0	10.6	286.0	10.6	60.0	75.0	150.0	0.0	240.0	15.0	14 /	12
124	79 320	74037	36.63	140.68	104.7	4.0	57.9	21.1	328.1	0.4	239.0	68.9	105.0	15.0	11.0	14.5	15 /	13
							0.5	50.8	154.4	36.3	254.1	13.0	105.0	75.0	345.9	7.4	15 /	13
125	79 4 1	221522	37.11	141.09	94.8	4.4	149.5	50.8	355.6	36.3	255.9	13.0	45.0	75.0	164.2	7.4	22 /	19
							119.0	10.6	211.0	10.6	345.0	75.0	75.0	0.0	165.0	15.0	22 /	19
126	79 611	1652 5	37.39	139.19	176.1	4.5	73.3	60.9	276.6	27.1	181.5	9.9	300.0	70.0	88.4	17.2	41 /	33
127	79 618	16 950	35.55	139.58	146.7	4.3	194.9	73.1	342.7	14.5	75.0	8.7	170.0	30.0	330.6	58.5	21 /	20
128	79 916	174812	36.32	138.36	177.1	4.4	250.0	85.0	70.0	5.0	340.0	0.0	70.0	50.0	250.0	40.0	26 /	23
129	791028	143933	35.06	140.94	92.2	5.5	9.2	68.3	244.4	12.8	150.3	17.2	50.0	30.0	266.1	54.5	142 /	127
130	7911 1	194554	37.64	141.55	82.2	4.1	71.6	66.7	293.2	17.8	198.4	14.5	315.0	60.0	101.3	25.7	10 /	10
							194.0	54.3	351.9	33.6	89.0	10.6	315.0	75.0	181.0	10.6	10 /	10
131	791125	191521	36.67	141.13	102.2	5.4	356.5	34.2	92.2	8.3	194.0	54.5	50.0	30.0	309.7	17.2	67 /	58
132	791217	1439 1	37.20	140.02	115.9	4.0	138.4	66.7	276.8	17.8	11.6	14.5	255.0	60.0	108.7	25.7	10 /	10
133	80 117	105218	32.83	142.07	110.0	5.5	233.1	55.4	332.8	6.6	67.2	33.8	180.0	30.0	300.8	41.6	62 /	48
134	80 3 6	20 451	32.85	140.13	114.8	4.8	217.4	51.0	76.6	32.1	333.6	19.7	240.0	10.0	124.5	67.7	61 /	54
135	80 312	122151	35.00	140.68	95.6	5.6	355.4	74.5	254.0	3.1	163.2	15.2	60.0	40.0	269.5	46.0	118 /	106
136	80 322	171640	38.75	141.05	84.0	4.2	28.4	35.0	122.1	5.2	219.4	54.5	340.0	20.0	81.2	28.0	12 /	12
137	80 323	235813	31.08	140.56	139.3	5.3	358.8	28.0	268.4	0.8	176.8	62.0	310.0	20.0	47.1	18.8	88 /	77
138	80 428	65913	38.41	140.64	105.3	4.3	326.2	73.9	127.3	15.3	218.7	5.0	120.0	60.0	311.5	29.5	14 /	13
139	80 6 5	215016	33.95	139.86	102.8	4.5	350.8	68.3	115.6	12.8	209.7	17.2	310.0	30.0	94.0	54.5	19 /	18
140	80 815	6 734	34.86	139.80	104.1	5.0	187.3	75.7	304.1	6.6	35.6	12.7	290.0	50.0	135.4	37.2	94 /	78
141	801020	122920	33.11	140.86	82.4	5.2	29.5	50.8	235.6	36.3	135.9	13.0	285.0	75.0	44.2	7.4	117 /	103
							164.0	54.3	321.9	33.6	59.0	10.6	285.0	75.0	151.0	10.6	117 /	103
142	801023	22123	35.99	138.94	145.0	4.1	16.0	90.0	285.0	0.0	195.0	0.0	285.0	45.0	105.0	45.0	16 /	16
143	8011 3	10 614	38.25	140.63	129.8	5.1	27.4	51.0	246.6	32.1	143.6	19.7	50.0	10.0	294.5	67.7	71 /	54
144	8012 7	183323	32.89	140.36	163.0	5.1	232.7	81.6	102.9	5.4	12.3	6.4	110.0	50.0	277.0	39.3	60 /	52

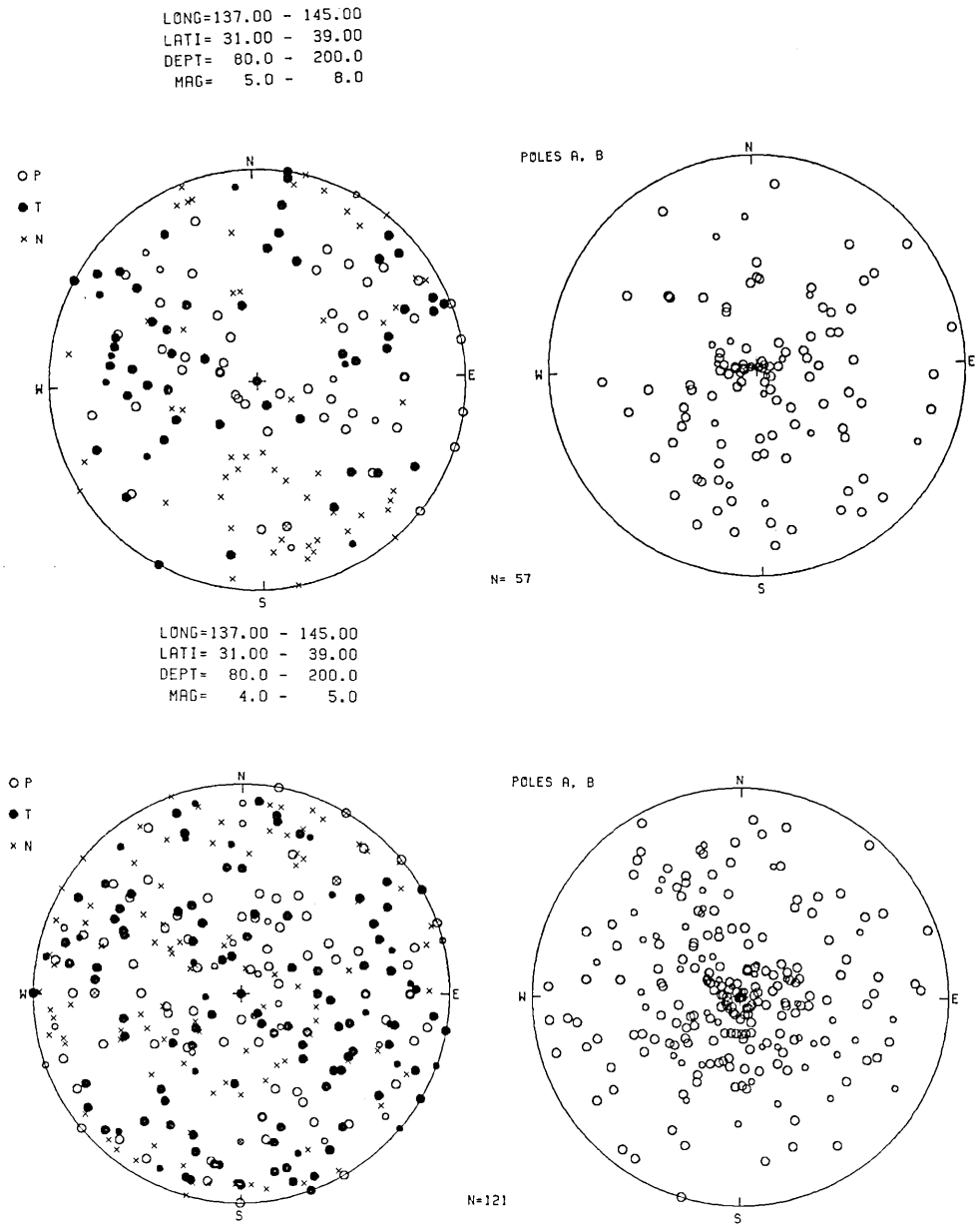

Fig. 15. Summary of fault-plane solutions of intermediate-depth earthquakes which occurred at depths of $h=80\sim200$ km with magnitudes of 4.0 or more in and around the Kanto District during the period from 1963 to 1980. (a) Equal-area projection of axes of maximum tension and compression and null vector denoted by empty and solid circles and crosses, respectively. (b) Equal-area projection of poles of nodal planes on the right-hand side. Smaller symbols denote multiple solutions for same earthquakes.

the Kanto District and vicinity. Smaller earthquakes show a wide variation of fault-plane solutions, which may be produced by the local stress. For such a region with complicated earthquake-generating stress, analyses using composite first-motion data may not be useful due to the mixed distribution of first-motion data for variable focal mechanisms. Individual focal mechanisms tend to exaggerate the spatial variations of earthquake-generating stress.

4. Spatial variation of focal mechanisms of intermediate-depth earthquakes

The occurrence of earthquakes in the Kanto District has a certain relationship with the intersection of three lithospheric slabs of the Pacific, Philippine Sea and overriding plates. The two systems of the Northeast Honshu and Izu-Bonin slabs show the contortion or disruption due to the different dipping angles beneath the Kanto District (ISACKS *et al.*, 1968; ISACKS and MOLNAR, 1971; UTSU, 1974). The lateral segmentation of the slab beneath Central Japan has also been suggested by the deep-focus earthquakes with the strike-slip (AOKI, 1974). FUJITA and KANAMORI (1981) excluded the Kanto region from the global survey of the double seismic zone due to the fact that its features are too complicated.

The geographical distribution of focal mechanisms is shown in Fig. 16 for 48 relatively large earthquakes of $M \geqq 5.0$. The greatest magnitude of 5.9 for these earthquakes is given to an earthquake which occurred off Miyagi Prefecture on Oct. 6, 1976 ($h = 91.2$ km). The westward plunging of P axes along the inclined seismic zone is observed for earthquakes on the western side and the westward dipping of T axes on the Pacific side. These features of focal mechanisms indicate the "down-dip" stresses along the inclined seismic zone (ISACKS and MOLNAR, 1971; HASEGAWA *et al.*, 1978a). Other types of focal mechanisms are also observed, such as the strike-slip, normal fault with the N-S extension, the northern or southern side sinking along the nearly vertical E-W plane, and the reverse fault with the E-W compression. These focal mechanisms include the effects of the "in-plane" stresses as pointed out by FUJITA and KANAMORI (1981). The nearly vertical E-W plane is produced by the hinge faulting or lateral segmentation of the descending slab. Such variable types of focal mechanisms suggest the spatial variation of earthquake-generating stress at intermediate-depths beneath the Kanto District and vicinity. Especially the different types of focal mechanisms from "down-dip" compression or extension are caused by the intersection of the two slabs.

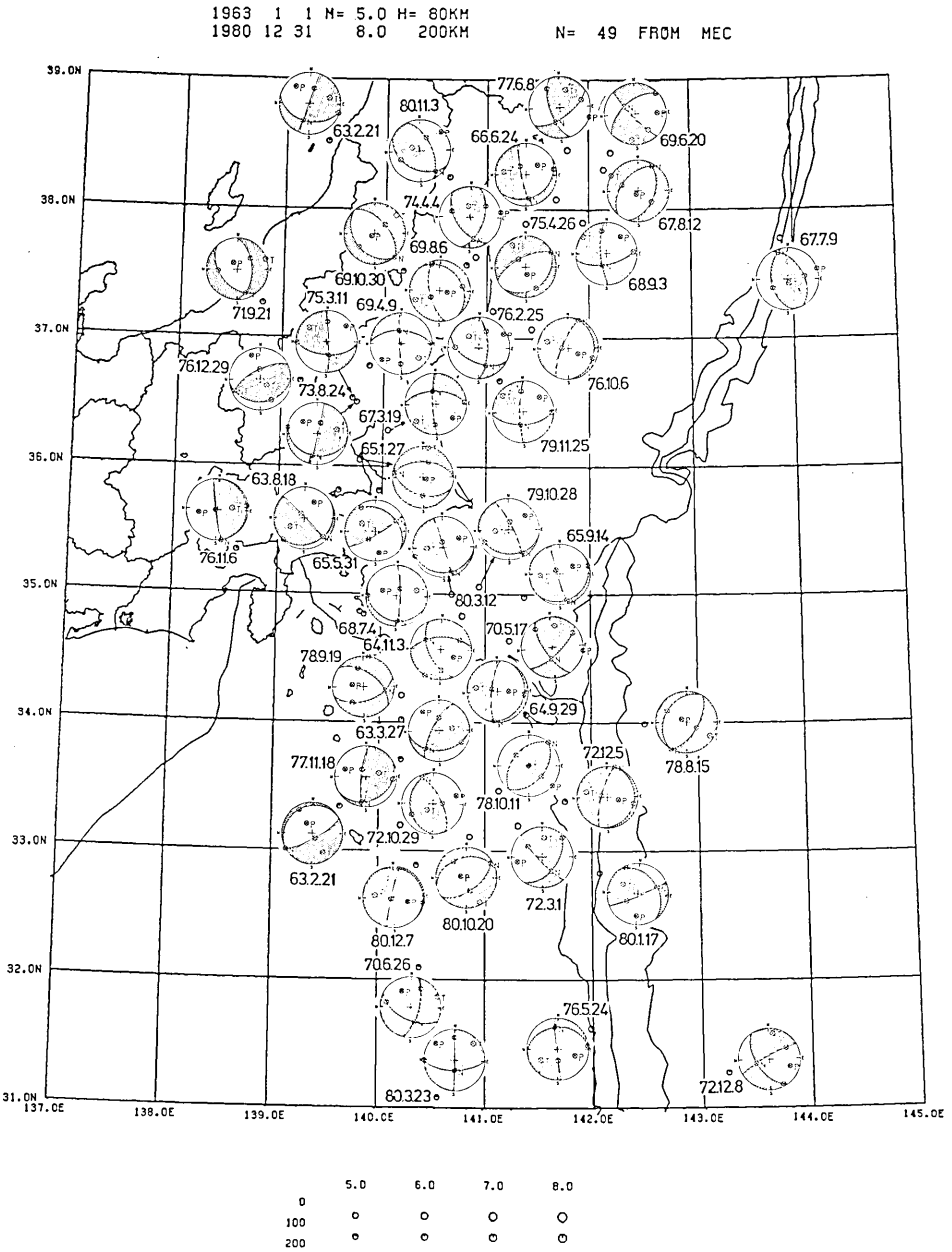

Fig. 16. Geographical dstribution of schematic diagrams (equal-area projection of the lower focal hemisphere) of focal mechanisms of intermediate-depth earthquakes which occurred at depths from 80 to 200 km with magnitudes of 5.0 or more in and around the Kanto District during the period from 1963 to 1980. Shaded and open areas of mechanism diagrams denote compressional and tensional areas of first motion, and the letters "P", "T" and "N" denote axes of maximum pressure and tension and null vector, respectively.

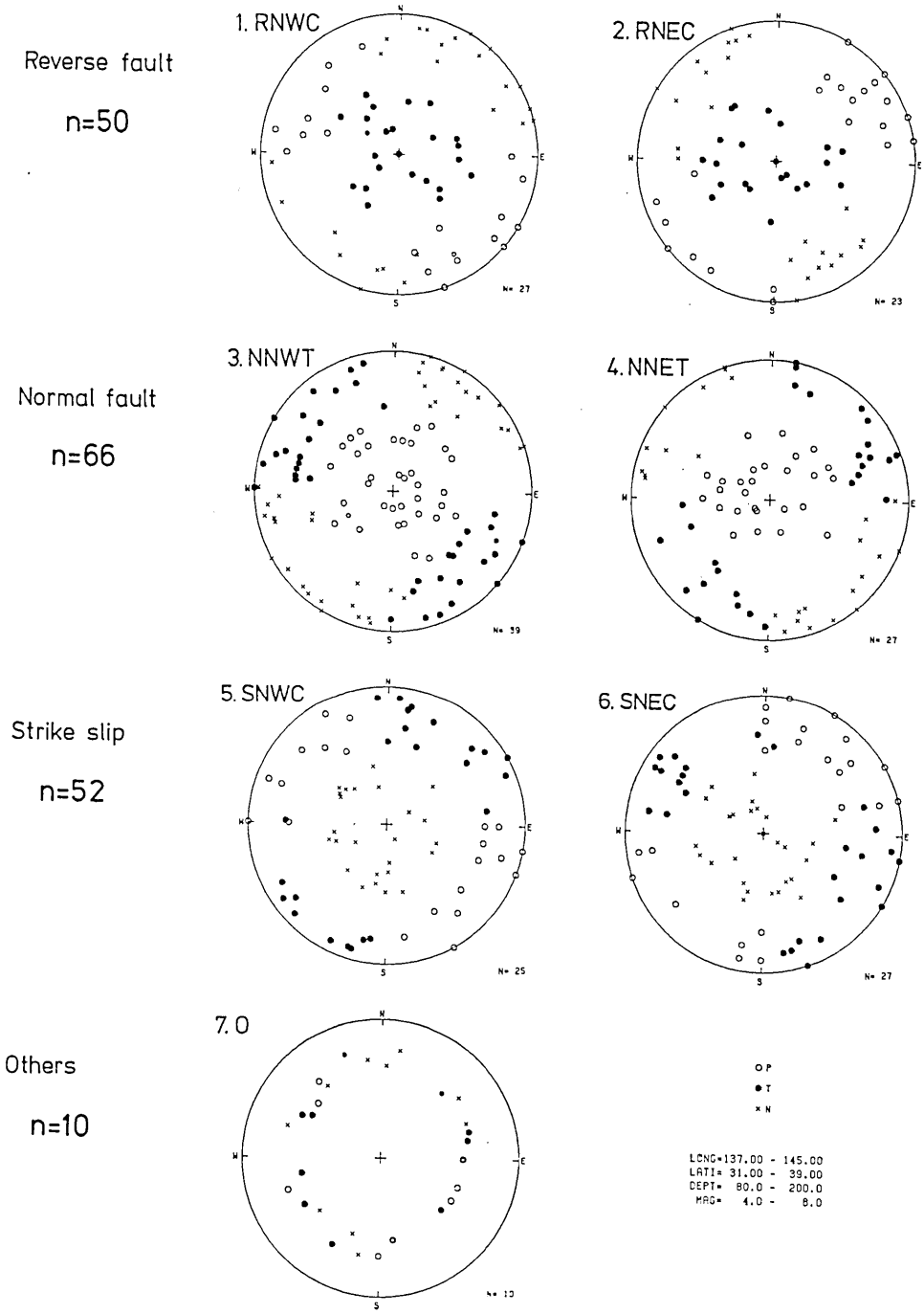

Fig. 17. Classification of fault-plane solutions of intermediate-depth earthquakes (h= 80~200 km) in and around Kanto District; (1) RNWC: reverse fault with the NW-SE compression, (2) RNEC: reverse fault with the NE-SW compression, (3) NNWT: normal fault with the NW-SE extension, (4) NNET: normal fault with the NE-SW extension, (5) SNWC: strike-slip with the NW-SE compression, (6) SNEC: strike-slip with the NE-SW compression, and (7) O: others. The numbers of solutions (n) are given for each type.

For detecting the fine spatial variation of focal mechanisms, fault-plane solutions are systematically classified by azimuths and dip angles of principal axes. Reverse, normal and strike-slip faults are identified by steeper dip angles of maximum tension and pressure and null vector, respectively. The 178 fault-plane solutions are classified into six types with equal parts, compared to the predominant reverse faults for shallower earthquakes (MAKI, 1983b). Fig. 17 shows seven types of fault-plane solutions for 144 intermediate-depth earthquakes; (1) reverse fault with the NW-SE compression (RNWC), (2) reverse fault with the NE-SW compression (RNEC), (3) normal fault with the NW-SE extension (NNWT), (4) normal fault with the NE-SW extension (NNET), (5) strike-slip with the NW-SE compression (SNWC), (6) strike-slip with the NE-SW compression (SNEC) and (7) others (O). Empty and solid circles denote axes of maximum pressure and tension, and crosses denote the null vector. The geographical distribution of fault types is represented in Fig. 18 by different symbols of epicenters as shown in the legend, namely solid and empty symbols for reverse and normal faults and crosses for strike-slips. Each type is separated into two groups based on azimuths of P or T axes for reverse or normal faults, and by P axes for strike-slips. Earthquake magnitudes are represented by different sizes of symbols. Compared to the shallower earthquakes normal faults and strike-slips are more frequently observed. The reverse faults are observed for earthquakes located beneath the Kanto District and in the coastal region on the Pacific side (MIYAGI and FUKUSHIMA Prefectures) and on the eastern side of the Izu-Bonin Islands. The normal faults are observed for earthquakes in the inland region on the Japan Sea side, off coast of Miyagi and Fukushima Prefectures, and near the Boso triple junction far east off the Boso Peninsula. The strike-slip faults are observed for earthquakes located just beneath the Kanto District, especially from Chiba to Yamanashi Prefecture (the hatched area in Fig. 18). Earthquakes at depths of $h=80\sim200$ km are generally located along the lower plane or within the seismic zone. Variable types of focal mechanisms are considered to be produced by the high stress level and lateral distortion of descending slabs due to the intersection of the two slabs beneath the Kanto District.

In Fig. 19 (a to f) the depth variations of mechanism types along the E-W sections are shown only for intermediate-depth earthquakes. For earthquakes with magnitudes of 5.0 or more, schematic diagrams of focal mechanism are shown using the equal-area projection of the northern focal hemisphere. The reverse faults (solid symbols) are observed for most of these earthquakes along the upper boundary of the inclined seismic zone, especially along the northern sections between

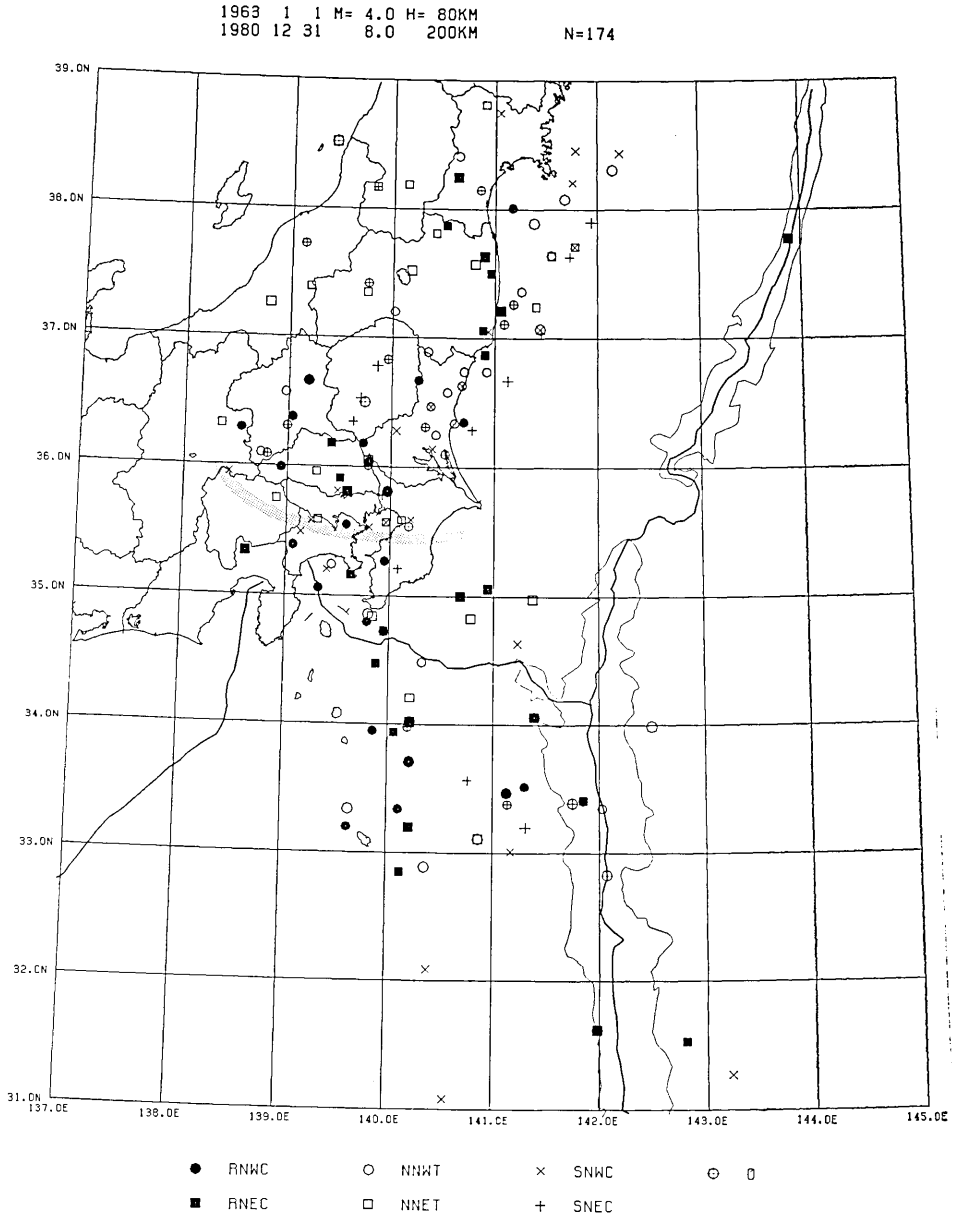

Fig. 18. Geographical distribution of the fault types of intermediate-depth earthquakes which occurred at depths of h=80~200 km with magnitudes of 4.0 or more in and around the Kanto District during the period from 1963 to 1980. Epicenters are represented by different symbols of fault types as shown in the legend. Reverse and normal faults are represented by solid and empty symbols, circles for the NW-SE stress and squares for the NE-SW stress, and strike-slips are shown by crosses, respectively.

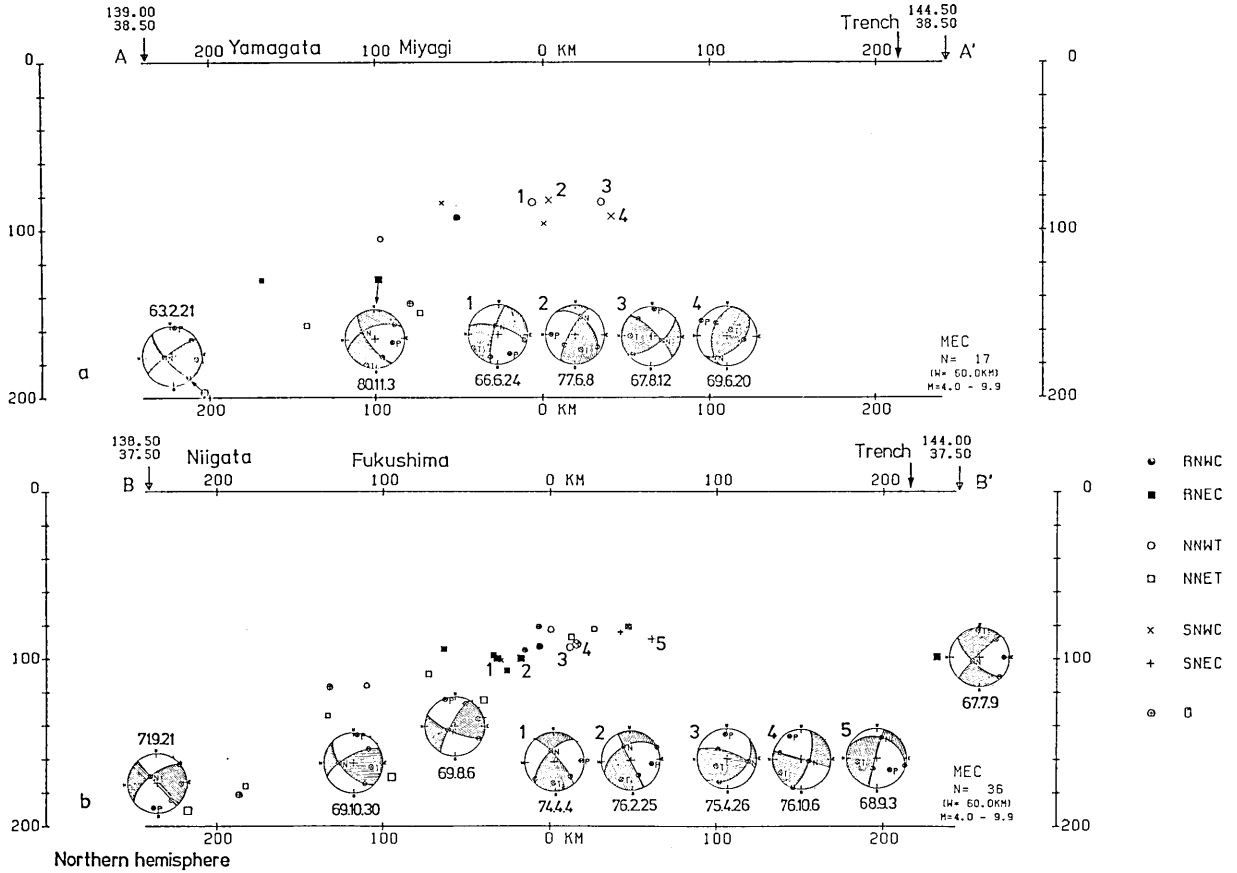
139.00
38.50
A
200 Yamagata
100 Miyagi
0 KM
100
200
Trench
144.50
38.50
A'
0
100
200
63.2.21
80.11.3
66.6.24
77.6.8
67.8.12
69.6.20
MEC
N= 17
(W= 60.0KM)
M=4.0 - 9.9
a
138.50
37.50
B
Niigata
Fukushima
Trench
144.00
37.50
B'
67.7.9
71.9.21
69.8.6
69.10.30
74.4.4
76.2.25
75.4.26
76.10.6
68.9.3
MEC
N= 36
(W= 60.0KM)
M=4.0 - 9.9
b
RNWC
RNEC
NNWT
NNET
SNWC
SNEC
Northern hemisphere

Fig. 19. a-b

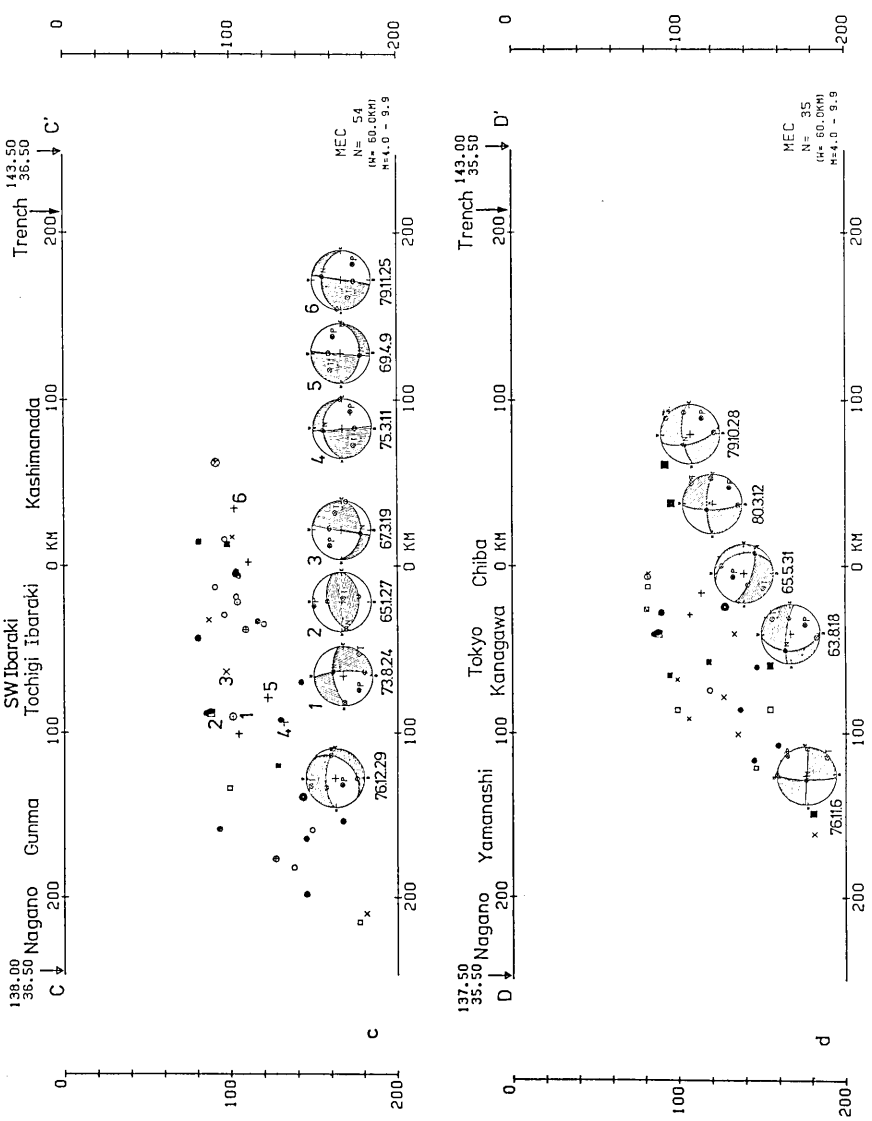
138.00
36.50
Nagano
Gunma
SW Ibaraki
Tochigi Ibaraki
Kashimanada
Trench
143.50
36.50
C
C'
0 KM
MEC
N= 54
(M= 60.0KM)
M=4.0 - 9.9
7612.29
73.824
651.27
67.319
75.311
69.4.9
791125
c
137.50
35.50
Nagano
Yamanashi
Tokyo
Kanagawa
Chiba
Trench
143.00
35.50
D
D'
MEC
N= 35
(M= 60.0KM)
M=4.0 - 9.9
76116
63.818
65.531
80.312
791028
d
ANHC
ANEC
NNHT
NNET
SNHC
SNEC
Northern hemisphere

Fig. 19. c–d

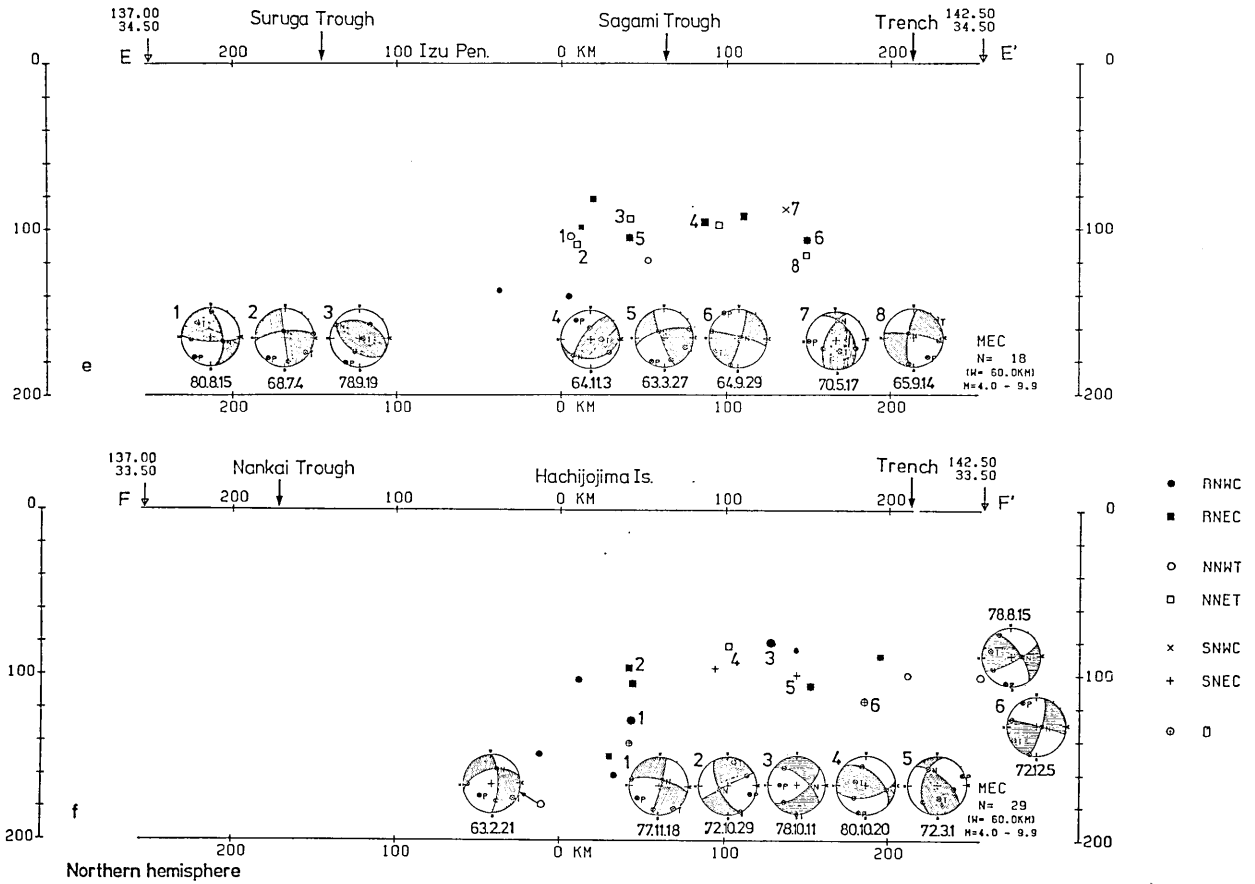

Fig. 19. Depth variation of fault types and equal-area projection of the northern focal hemisphere for intermediate-depth earthquakes along the E-W sections between the following two points; (a) A(38.5°N, 139.0°E) and A′(38.5°N, 144.5°E), (b) B(37.5°N, 138.5°E) and B′(37.5°N, 144.0°E), (c) C(36.5°N, 138.0E) and C′(36.5°N, 143.5°E), (d) D(35.5°N, 137.5°E) and D′(35.5°N, 143.0E), (e) E(34.5°N, 137.0°E) and E′(34.5°N, 142.5°E) and (f) F(33.5°N, 137.0°E) and F′(33.5°N, 142.5°E). Fault-plane solutions are classified into seven types as shown in Figs. 17 and 18. Schematic diagrams of the northern focal hemisphere are represented only for earthquakes with magnitudes of 5.0 or more.

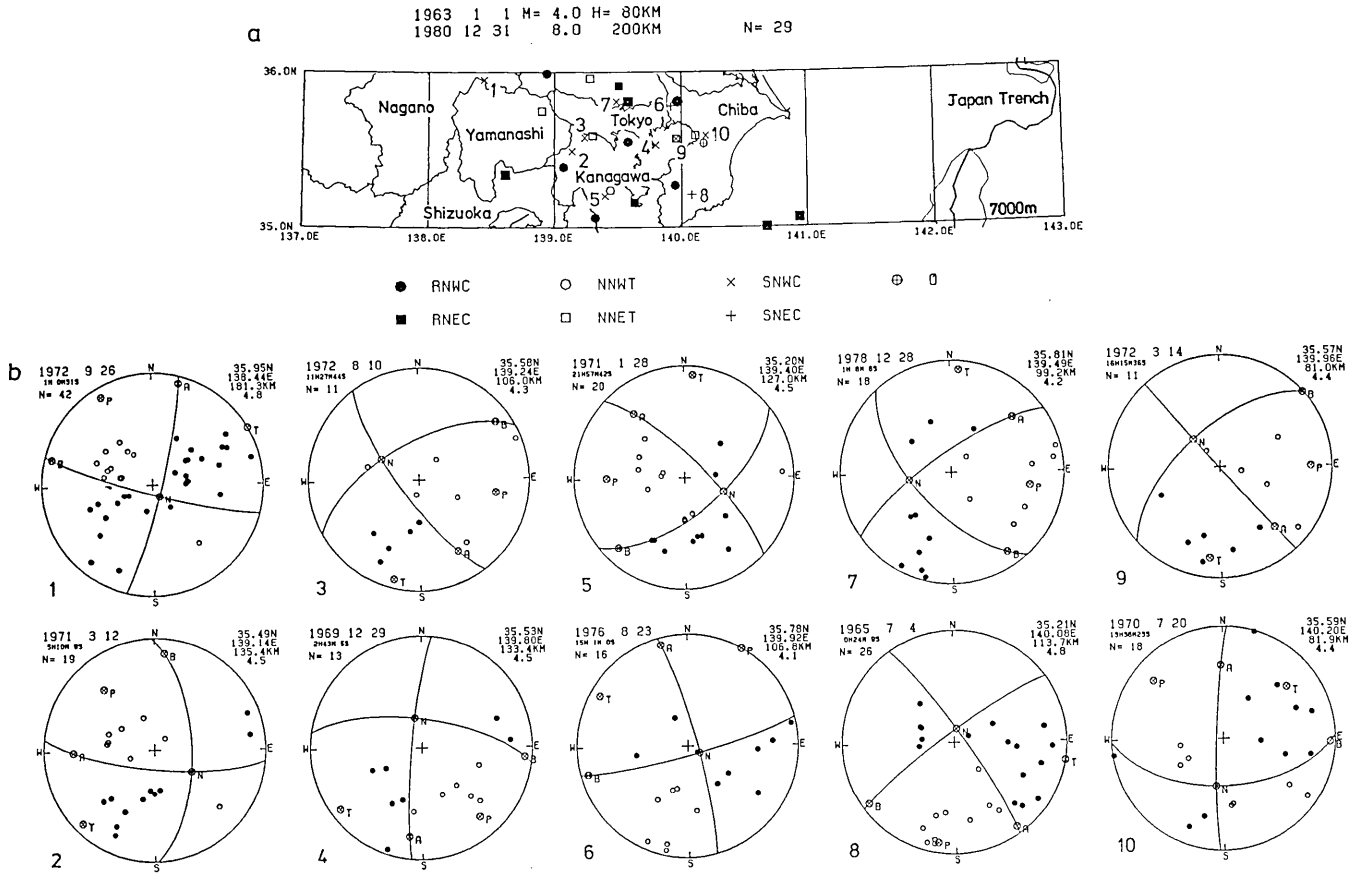

Fig. 20. Enlargement of the geographical distribution of fault types beneath the central part (around the 36°N line) of the Kanto District, where the strike-slip faults are predominant (a), and the equal-area projection of the lower focal hemisphere of focal mechanisms and first-motion data (b). Epicenters and fault-plane solutions are referred by earthquake numbers.

37° to 35°N (CC′ and DD′). A lower plane of the inclined seismic zone with a separation of about 30 km is observed for the E-W sections from 36° to 37°N. The reverse faults along the upper plane of the inclined seismic zone are observed for earthquakes at depths down to 80 km (MAKI, 1983b). The down-dip extension along the lower plane of the double seismic planes is disturbed and other types of focal mechanisms are observed beneath the Kanto District.

Fig. 20 shows an enlargement of the central part of the Kanto District, where the strike-slip faults are predominant. The upper part denotes epicenters classified by mechanism types, and the lower part shows the equal-area projection of the lower focal hemisphere and first-motion data for 10 earthquakes with strike-slips. Alternate directions of silp motions along the nearly E-W plane suggest complicated slippages along the contact plane. These types of focal mechanism and the acute depth contours suggest the deep-seated fracture zone between the Northeast Honshu and Izu-Bonin slabs. This fracture zone may be extended to the source region of the Takayama deep-focus earthquakes with the strike-slip in the deeper part (ISACKS *et al.*, 1968; AOKI, 1974), and in the shallower part to a disturbed trench axis showing the discontinuous bathymetric contours of 7000 m.

Spatial variations of focal mechanisms of intermediate-depth earthquakes were studied using individual solutions of relatively large earthquakes, mechanism types classified by axes of principal stresses, and summaries of fault-plane solutions. Compared to the predominant reverse faults along the upper plane of the inclined seismic zone, the earthquakes located within the seismic zone show variable types of focal mechanisms, including the normal faults and strike-slips. Strike-slip faults are seen for earthquakes located directly beneath the Kanto District and may be explained by the northwestward bending of the Northeast Honshu slab and contact with the Izu-Bonin slab. The earthquakes located around the Izu-Bonin Islands show more variable types of focal mechanisms.

5. Discussion and conclusion

The precise relocated hypocenters in the Kanto District and vicinity were obtained using the JMA travel-time data by correcting the Pn station biases (MAKI, 1981a). Microearthquakes in the Kanto District and Northeast Japan are located through the preliminary determination of origin times using S-P times observed at nearby stations. SUZUKI *et al.* (1981) compared the differences of hypocenters located by the preliminary determination of origin times from the S-P times and by using only the P times. The double seismic zone was even

observed by the P wave travel-time data (MAKI, 1981), especially by the JHD method (MAKI, 1979).

The descending slab of the Pacific Plate beneath Northeast Honshu and the Izu-Bonin Islands is outlined from the epicenter maps of intermediate-depth earthquakes for the different ranges of focal depth. The upper plane of the inclined seismic zone, which can be located by the western extremities of epicenters, shows a gentle dip of 30° beneath Northeast Honshu and the steeper dip of 60° beneath the Izu-Bonin Islands. Depth contours show the acute curve beneath Central Japan. These contorted depth contours suggest the complicated intersection of the northern end of the Izu-Bonin slab and the southwestern end of the Northeast Honshu slab. The northwestward bending at the shallower part and the disruption at the deeper part beneath Central Honshu have been shown by ISACKS *et al.* (1974). Some seismically active regions are observed in the shallower part where the greater stress is stored due to the strong bending of the Northeast Honshu slab and the intersection of the two slabs. The northwestward bending beneath Central Japan is consistent with the Quarternary compressive deformation and Miocene terrains (MATSUDA, 1978), volocanic front (SUGIMURA, 1960) and metamorphic belts (MIYASHIRO, 1961).

Fault-plane solutions ($n=178$) were obtained by the numerical method for about a half (144 out of 286) of intermediate-depth earthquakes which occurred during the period from 1963 to 1980 with magnitudes of 4.0 or more. In general, the intermediate-depth earthquakes located along the upper plane of the inclined seismic zone show the focal mechanisms of the down-dip compression, while those located along the lower plane show a focal mechanism of down-dip extension. Besides the two types of mechanisms related to the double seismic planes, a variety of focal mechanisms, including the strike-slip, hinge fault along the vertical E-W plane and normal fault with the N-S compression, have been observed, especially along the lower part of the inclined seismic zone. The strike-slip is observed for earthquakes located directly beneath the Kanto District and it seems to be related to the contact plane of southwestern end of the Northeast Honshu slab and the northern end of the Izu-Bonin slab. The alternate directions of slip motions along the nearly E-W striking plane suggest the complicated slippages of the two descending slabs.

Fig. 21 represents a tentative model showing the intersection of the Northeast Honshu and Izu-Bonin slabs beneath Central Japan by the perspective projection viewed at an altitude of 100 km over the Japan Sea (40°N, 136°E) towards the point (36°N, 140°E). Shore lines and trench axes are also actually shown, and depth contours of upper boundary of the seismic zone are denoted by thick lines for every 20

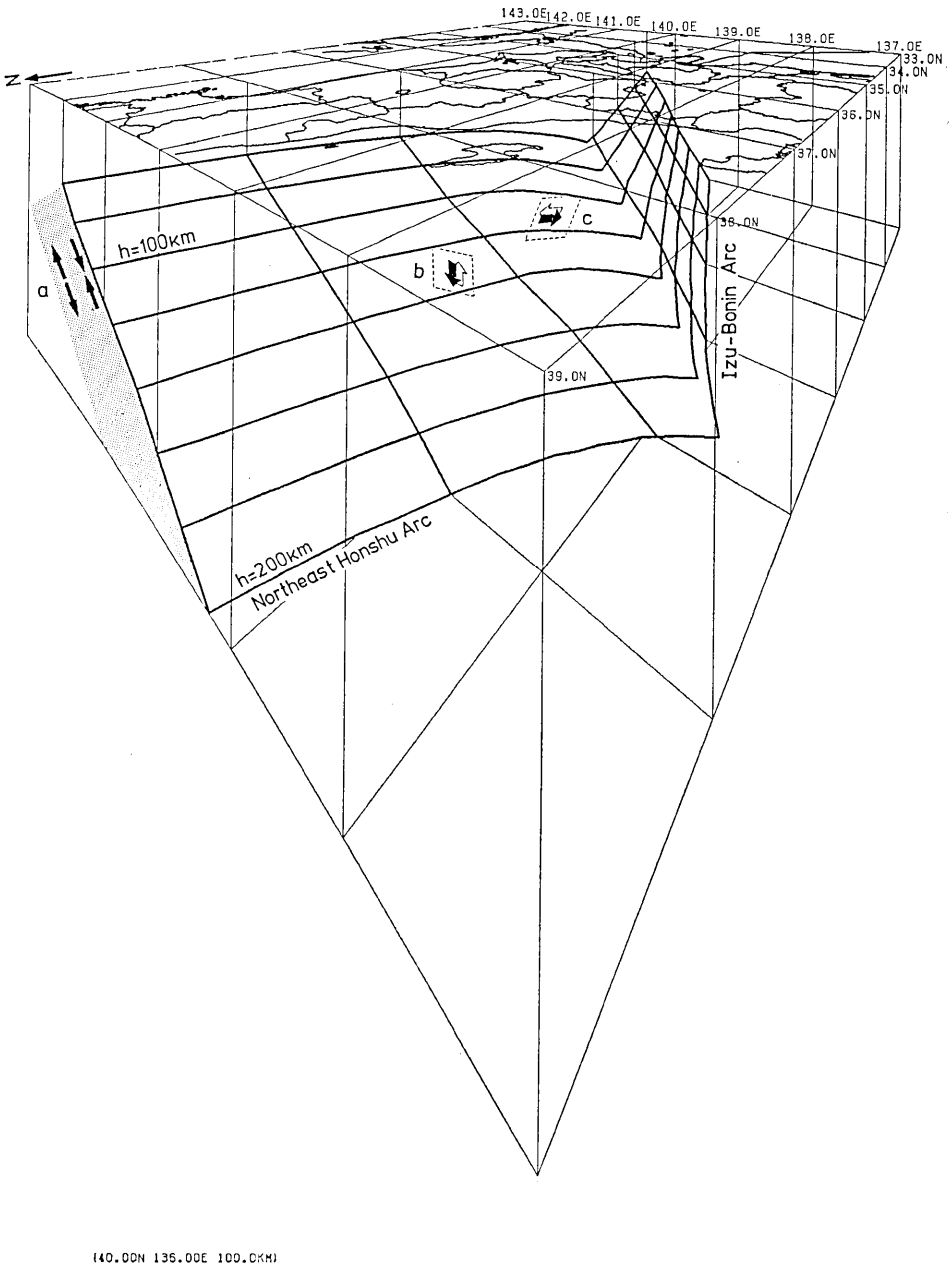

Fig. 21. Perspective view of intersection of the Northeast Honshu and Izu-Bonin slabs viewed from an altitude of 100 km over the Japan Sea (40°N, 136°E) toward the point (36°N, 140°E). The inclined seismic zones are derived based on the depth contours for every 20 km from 60 to 200 km in Fig. 5. Some fault types are shown at arbitrary locations, (a) the down-dip compression and extension along the inclined seismic zone (a hatched zone), (b) the hinge fault, and (c) the strike-slip related to the contact of the Northeast Honshu and Izu-Bonin slabs.

km of depths from 60 to 200 km. The gentle dipping of 30° for the Northeast Honshu slab and the steeper dip of 60° for the Izu-Bonin slab are shown. Some types of focal mechanisms are shown, (a) the down-dip compression and extension along the inclined seismic zone (shaded area), (b) the hinge fault along the vertical plane striking nearly E-W, and (c) the strike-slip along the contact plane between the Northeast Honshu and Izu-Bonin slabs. The reverse fault with the N-S compression is obtained for the Middle Saitama Earthquake on July 1, 1968 ($h=60.8$ km, M 6.1) as well as ABE (1975). This earthquakes is located on the northward dipping plane of the northwestern end of the Northeast Honshu slab. Portions shallower than 60 km are excluded in this representation. Intensely active regions beneath the Kanto District are located within the intersecting region of the Northeast Honshu and Izu-Bonin slabs. A separation of focal mechanisms into the down-dip compression and extension is observed in Northeast Japan. Such a simple separation is produced by the descent of the single slab which is independent of the effects of the adjacent slabs of the Kurile and Izu-Bonin Arcs.

Features of the double seismic zone vary from section to section in and around the Kanto District. For the northern sections the spatial distribuion of hypocenters and focal mechanisms show a simple pattern of the double seismic planes, but for the southern sections even the inclined patterns of the seismic zone cannot be easily observed. Such variations between the northern and southern sections are caused by the effect of intersection of two slabs with the different coupling between the Pacific Plate and overriding plates (KANAMORI, 1971, 1977; KELLEHER and MCCANN, 1976; UYEDE and KANAMORI, 1979). Further studies are necessary for the fine structure of the spatial distribution of hypocenters and focal process of intermediate-depth earthquakes.

Acknowledgements

The author would like to acknowledge Profs. Tokuji Utsu and Kazuaki Nakamura for reviewing the manuscript. Helpful comments are also acknowledged from Dr. Sadaomi Suzuki of Hokkaido University, and from the members of the Utsu Seminar on Jul. 5, 1983. He thanks Prof. Tsumura and coworkers for the use of the ERI Hypocenter Data and the Seismological Section of JMA for the use of the Data File of the travel-times. Dr. Norihito Umino of Tohoku University kindly transferred the Veith's Ph. D. Thesis. Computations and drafting were made by using the IBM 4341 of the Earthquake Prediction Data Center, Earthquake Research Institute, Uni-

versity of Tokyo.

References

ABE, K., 1975, Static and dynamic fault parameters of the Saitama Earthquake of July 1, 1968, *Tectonophysics*, **27**, 223-238.

AOKI, H., 1974, Plate tectonics of arc-junction at Central Japan, *Journ. Phys. Earth*, **22**, 141-161.

BARAZANGI, M. and B. L. ISACKS, 1979, A comparison of the spatial distribution of mantle earthquakes determined from data produced by local and by teleseismic networks for the Japan and Aleutian arcs, *Bull. Seism. Soc. Amer.*, **69**, 1763-1770.

CARDWELL, R.K. and B.L. ISACKS, 1978, Geometry of the subducted lithosphere beneath the Banda Sea in Eastern Indonesia from seismicity and fault plane solutions, *Journ. Geophys. Res.*, **83**, 2825-2838.

DOREL, J., 1981, Seismicity and seismic gaps in the Lesser Antilles arc and earthquake hazard in Guadeloupe, *Geophys. Journ. Roy. astr. Soc.*, **67**, 679-696.

ENGDAHL, E.R. and C.H. SCHOLZ, 1977, A double Benioff zone beneath the central Aleutian: An unbending of the lithosphere, *Geophys. Res. Lett.*, **4**, 473-476.

FORSYTH, D. W., 1975, Fault plane solutions and tectonics of the South Atlantic and Scotia Sea, *Journ. Geophys. Res.*, **80**, 1429-1443.

FUJITA, K. and H. KANAMORI, 1981, Double seismic zones and stresses of intermediate depth earthquake, *Geophys. Journ. Roy. astr. Soc.*, **66**, 131-156.

GOTO, K. and H. HAMAGUCHI, 1983, Characteristics of distributions of thermal stress and stress due to phase change in the descending plate beneath island arcs, *Zishin* II, **36**, 31-41 (in Japanese).

HASEGAWA, A., N. UMINO and A. TAKAGI, 1978a, Double-planed structure of the deep seismic zone in the northeastern Japan arc, *Tectonophysics*, **47**, 43-58.

HASEGAWA, A., N. UMINO and A. TAKAGI, 1978b, Double-planed deep seismic zone and upper-mantle structure in the Northeastern Japan Arc, *Geophys. Journ. Roy. astr. Soc.*, **54**, 281-296.

HASEGAWA, A., N. UMINO, A. TAKAGI and Z. SUZUKI, 1979, Double-planed deep seismic zone and anomalous structure in the upper mantle beneath Northeastern Honshu (Japan), *Tectonophysics*, **57**, 1-6.

ICHIKAWA, M. and E. MOCHIZUKI, 1971, Travel time tables for local earthquakes in and near Japan, *Papers Meteorol. Geophys.*, **22**, 229-290 (in Japanese).

ISACKS, B.L. and M. BARAZANGI, 1977, Geometry of Benioff zone: Lateral segmentation and downwards bending of the subducted lithosphere, in "*Island Arcs, Deep Sea Trenches and Back-Arc Basins*", Maurice Ewing Ser., vol. 1, edited by M. TALWANI and W. C. PITMAN III, AGU, Washington, D. C., pp. 99-114.

ISACKS, B. L. and P. MOLNAR, 1971, Distribution of stresses in the descending lithosphere from a global survey of focal mechanism solution of mantle earthquakes, *Rev. Geophys. Space Phys.*, **9**, 107-170.

ISACKS, B. L., L. R. SYKES and J. OLIVER, 1968, Focal mechanisms of deep and shallow earthquakes in the Tonga-Kermadec region and the tectonics of islands arcs, *Bull. Geol. Soc. Amer.*, **80**, 1443-1470.

KANAMORI, H., 1971, Great earthquakes at island arcs and the lithsphere, *Tectonophysics*, **12**, 187-198.

KANAMORI, H., 1977, Seismic and aseismic slip along subduction zones and their tectonic implications, in "*Island Arcs, Deep Sea Trenches and Back-Arc Basins*", Maurice Ewing Ser., vol. 1, edited by M. TALWANI and W.C. PITMAN III, AGU, Washington, D. C., pp. 162-174.

KATSUMATA, M. and L.R. SYKES, 1969, Seismicity and tectonics of the western Pacific: Izu-

Mariana-Caroline and Ryukyu-Taiwan region, *Journ. Geophys. Res.*, **74**, 5923-5948.
KELLEHER, J. and W. MCCANN, 1976, Buoyant zones, great earthquakes, and unstable boundaries of subduction, *Journ. Geophys. Res.*, **81**, 4885-4896.
MAKI, T., Joint hypocenter determination of earthquakes in the Kanto District, Read on May 4, 1979, at the semi-annual meeting of the Seismological Society of Japan.
MAKI, T., 1981a, Regional variation of Pn residuals and its application to relocation of earthquakes in and around the Kanto District, *Bull. Earthq. Res. Inst.*, **56**, 309-346.
MAKI, T., 1981b, Earthquake mechanisms of subcrustal earthquakes beneath the Kanto District, *Memoirs Geol. Soc. Japan*, **20**, 259-266 (in Japanese).
MAKI, T., 1982a, Effects of observational conditions on hypocenter location of intermediate-depth earthquakes in Central Japan, *Bull. Earthq. Res. Inst.*, **57**, 49-82.
MAKI, T., 1982b, Numerical estimation of confidence region of fault-plane solutions, *Bull. Earthq. Res. Inst.*, **57**, 193-220.
MAKI, T., 1983a, Extended travel-time tables for the JMA standard model of the crust and upper mantle structure beneath the Japanese Islands, *Bull. Earthq. Res. Inst.*, **58**, 311-383.
MAKI, T., 1983b, Spatial variation of earthquake-generating stresses in and around the Kanto District, Central Japan, *Bull. Earthq. Res. Inst.*, **58**, 591-646.
MAKI, T., I. KAWASAKI and A. HORIE, 1980, Earthquake mechanisms associated with the conjunction of the sinking plates beneath the Kanto District, Central Japan, *Bull. Earthq. Res. Inst.*, **55**, 577-600.
MAKI, T. and K. TSUMURA, 1980, On seismic fault-systems derived from the spatial distribution and mechanisms of the earthquakes in the Kanto District, *Journ. Anal. Res. Data Natur. Disast.*, **7**, 47-60 (in Japanese).
MATSUDA, T., 1978, Collision of the Izu-Bonin Arc with Central Honshu: Cenozoic tectonics of the Fossa Magna, *Journ. Phys. Earth*, **26**, *Suppl.*, s409-s421.
MIYASHIRO, A., 1961, Evolution of metamorphic belt, *Journ. Petr.*, **2**, 277-311.
MIZOUE, M., I. NAKAMURA, T. YOKOTA, H. CHIBA, M. YOSHIDA and H. HAGIWARA, Read on Apr. 8, 1981, at the semi-annual meeting of the Seismological Society of Japan.
MORIYA, T., 1978, Seismic studies of the upper mantle beneath the arc-junction at Hokkaido: Folded structure of intermediate-depth seismic zone and attenuation of seismic waves, *Journ. Phys. Earth*, **26**, *Suppl.*, s467-s475.
NISHIDE, N., M. YAMAMOTO and N. HAMADA, Read on Oct. 6, 1982, at the semi-annual meeting of the Seismological Society of Japan.
OKADA, H., 1971, Forerunners of ScS waves from nearby deep earthquakes and upper mantle structure in Hokkaido, *Zishin* II, **24**, 228-239 (in Japanese).
OKADA, H., 1979, New evidences of the discontinuous structure of the descending lithosphere as revealed by ScSp phase, *Journ. Phys. Earth*, **27**, *Suppl.*, s53-s63.
PASCAL, G., B.L. ISACKS, M. BARAZANGI and J. DUBOIS, 1978, Precise relocations of earthquakes and seismotectonics of the New Hebrides Island Arc, *Journ. Geophys. Res*, **83**, 4957-4973.
REYNERS, M. and K.S. COLES, 1982, Fine structure of the dipping seismic zone and subduction mechanics in the Shumagin Islands, Alaska, *Journ. Geophys. Res.*, **87**, 356-366.
SAMOWITZ, I.R. and D.W. FORSYTH, 1981, Double seismic zone beneath the Mariana Island Arc, *Journ. Geophys. Res.*, **86**, 7013-7021.
SASATANI, T., 1976, Mechanism of mantle earthquakes near the junction of the Kurile and the Northern Honshu Arcs, *Journ. Phys. Earth*, **22**, 141-161.
SHIONO, K., T. MIKUMO and Y. ISHIKAWA, 1980, Tectonics of the Kyushu-Ryukyu Arc as evidenced from seismicity and focal mechanism of shallow to intermediate-depth earthquakes, *Journ. Phys. Earth*, **28**, 17-43.
SLEEP, N.H., 1979, The double seismic zone in downgoing slabs and the viscosity of the mesosphere, *Journ. Geophys. Res.*, **84**, 4565-471.
STAUDER, W., 1973, Mechanism and spatial distribution of Chilean earthquakes with relation

to subduction of the oceanic plate, *Journ. Geophys. Res.*, **78**, 5033-5061.

STAUDER, W., 1975, Subduction of the Nazca Plate under Peru as evidenced by focal mechamnisms and by seismicity, *Journ. Geophys. Res.*, **80**, 1053-1064.

STAUDER, W. and L. MUALCHIN, 1976, Fault motion in the large earthquakes of the Kurile-Kamchatka Arc and of the Kurile-Hokkaido Corner, *Journ. Geophys. Res.*, **81**, 297-308.

STEFANI, J.P., R.J. GELLER and G.C. KROEGER, 1982, A direct measurement of the distance between a hypocenter in a Benioff-Wadati zone and the slab-asthenosphere contact, *Journ. Geophys. Res.*, **87**, 323-328.

STEIN, S., J.F. ENGELN, D.A. WIENS, K. FUJITA and R.C. SPEED, 1982, Subduction seismicity and tectonics in the Lesser Antilles Arc, *Journ. Geophys. Res.*, **87**, 8642-8664.

SUGIMURA, A., 1960, Zonal arrangement of some geophysical and petrological features in Japan and its environs, *Journ. Fac. Sci., Univ. Tokyo*, II, **12**, 133-153.

SUGIMURA, A. and S. UYEDA, 1973, "*Island Arcs—Japan and its environs*", 235 pp, Elsevier, Amsterdom.

SUZUKI, S., T. SASATANI and Y. MOTOYA, Read on Apr. 7, 1981, at the semi-annual meeting of the Seismological Society of Japan.

SUZUKI, S., T. SASATANI and Y. MOTOYA, 1983, Double seismic zone beneath the middle of Hokkaido, Japan, in the southwestern side of the Kurile arc, *Tectonophysics*, **96**, 59-76.

TAKAGI, A., A. HASEGAWA and N. UMINO, 1977, Seismic activity in the Northeastern Japan Arc, *Journ. Phys. Earth*, **25**, *Suppl.*, s95-s104.

TSUMURA, K., 1973, Microearthquake activity in the Kanto District, Publication for the 50th anniversary of the Great Kanto Earthquake, 1923, Earthq. Res. Inst., 67-87 (in Japanese).

TSUMURA, K., 1981, Spatial distribution of microearthquakes and larger earthquakes in the Kanto District, *Memoirs Geol. Soc. Japan*, **20**, 7-20 (in Japanese).

TSUMURA, K. and I. KARAKAMA, Read on Oct. 7, 1981, at the semi-annual meeting of the Seismological Society of Japan.

UKAWA, M. and M. IMOTO, Read on Oct. 6, 1982, at the semi-annual meeting of the Seismological Society of Japan.

UMINO, N. and A. HASEGAWA, 1975, On the two-layered structure of deep seismic plane in Northeastern Japan Arc, *Zishin* II, **28**, 125-139 (in Japanese).

UMINO, N. and A. HASEGAWA, 1982, A detailed structure of the deep seismic zone and earthquake mechanism in the Northeast Japan Arc, *Zishin* II, **35**, 237-257 (in Japanese).

UTSU, T., 1974, Hypocenter distribution in and near Japan, *Kagaku*, **44**, 739-746 (in Japanese).

UYEDA, S. and H. KANAMORI, 1979, Back-arc opening and the mode of subduction, *Journ. Geophys. Res.*, **84**, 1049-1061.

VEITH, K.F., 1974, The relationship of island arc seismicity to plate tectonics, Ph. D. Thesis of Southern Methodist University, 162 pp.

VEITH, K.F., 1977, The nature of the dual zone of seismicity in the Kuriles Arc, *Trans. Amer. Geophys. Union*, **58**, 1232.

YOSHII, T., 1979, A detailed cross-section of the deep seismic zone beneath Northeastern Honshu, Japan, *Tectonophysics*, **55**, 349-360.

島弧接合部における稍深発地震の震源分布と発震機構
——関東地方周辺の2層地震面——

東京大学地震研究所　牧　　正

関東地方周辺下においてもぐりこむスラブの形状と地震メカニズムについてしらべた．用いた震源は気象庁走時データに Pn 走時残差の観測点補正を行い決定したものであり，深さ別震央分布図，東西・南北に沿った深さ分布図からスラブ上面のコンターを求めた．東北日本弧は関東地方下で北西方向に彎曲しつつ伊豆小笠原弧と接合し，この彎曲は火山・変成岩帯の配列とも調和する．茨城県南西部・千葉県中部にみられる地殻下地震の高活動域は東北日本・伊豆小笠原弧の接合による高歪力部に位置している．今回用いた比較的大きな地震についても西側に傾むき下がる深発地震帯が2層に分離している．この2層構造は東北日本弧で明瞭であるが，伊豆小笠原弧では不鮮明である．JHD 法によって求められた高精度震源の深さ分布から，2 層面の間隔は 30 km である．深さ 80～200 km，$M \geq 4.0$, 1963～1980 年の期間に起こった関東地方と周辺の稍深発地震 286 個のうち 144 個に対して，初動方向データ 10 個以上を満足するメカニズム解が数値解法で求められた．逆断層又は地震面に沿った張力のメカニズムは太平洋側に，内陸側には地震面に沿った圧力のメカニズムがみられる．地震面に沿った歪力によるこれら2つのタイプの他，横ずれ・正断層・断裂のタイプもみられ，特に東北日本弧の南西端が伊豆小笠原弧の北端と接する部分では多くみられる．関東地方周辺の稍深発地震の起こり方として，2 層面構造によるもの，東北日本伊豆小笠原弧の接合に関連するもの，又各々のスラブ内の過程（断裂など）によるものなど多様な起こり方をしている．